

Pearson-Readhead Survey Sources II: The Longterm Centimeter-band Total Flux and Linear Polarization Properties of a Complete Radio Sample

M. F. Aller, H. D. Aller, and P. A. Hughes

*Department of Astronomy, University of Michigan, 817 Dennison Building, Ann Arbor, MI
48109-1090*

`margo,hugh,hughes@astro.lsa.umich.edu`

ABSTRACT

Using UMRAO centimeter-band total flux density and linear polarization monitoring observations of the complete Pearson-Readhead extragalactic source sample obtained between August 1984 and March 2001, we identify the range of variability in extragalactic objects as functions of optical and radio morphological classification, and relate total flux density variations to structural changes in published coeval VLBI maps in selected objects. As expected, variability is common in flat or inverted spectrum ($|\alpha| \leq 0.5$) core-dominated QSOs and BL Lacs. Unexpectedly, we find flux variations in several steep-spectrum sample members, including the commonly adopted flux standard 3C 147. Such variations are characteristically several-year rises or declines, or infrequent outbursts, requiring long-term observations for detection: we attribute them to the brightening of weak core components, a change which is suppressed by contributions from extended structure in all but the strongest events, and identify a wavelength-dependence for the amplitude of this variability consistent with the presence of opacity in some portions of the jet flow. One morphological class of steep-spectrum objects, the compact symmetric objects, characteristically shows only low-level variability. We examine the statistical relation between fractional polarization and radio class based on the data at 14.5 and 4.8 GHz. The blazars typically exhibit flat to inverted polarization spectra, a behavior attributed to opacity effects. Among the steep spectrum objects, the lobe-dominated FR Is have steep fractional polarization spectra; while the FR IIs exhibit fractional polarization spectra ranging from inverted to steep, with no identifiable common property which accounts for the range in behavior. For the cso/GHz-peaked-spectrum sources we verify that the fractional polarizations at 4.8 GHz are only of order a few tenths of a percent; but at 14.5 GHz we find significantly higher

polarizations, ranging from one to three percent; this frequency dependence supports a scenario invoking Faraday depolarization by a circumnuclear torus. We have identified preferred orientations of the electric vector of the polarized emission at 14.5 and 4.8 GHz in roughly half of the objects, and compared these with orientations of the flow direction indicated by VLBI morphology. When comparing the distributions of the orientation offsets for the BL Lacs and for the QSOs, we find differences in both range and mean value, in support of intrinsic class differences. In the shock-in-jet scenario, we attribute this to the allowed range of obliquities of shocks developing in the flow relative to the flow direction: in the BL Lacs the shocks are nearly transverse to the flow direction while in the QSOs they include a broader range of obliquities and can be at large angles to it. The fact that we find longterm stability in EVPA over many events implies that a dominant magnetic field orientation persists; in the core-dominated objects, with small contribution from the underlying quiescent jet, this plausibly suggests that the magnetic field has a longterm memory, with subsequent shock events exhibiting similar EVPA orientation, or, alternatively, the presence of a standing shock in the core. We have looked for systematic, monotonic changes in EVPA which might be expected in the emission from a precessing jet, a model currently invoked for some AGNs; none were identified. Further, we carried out a Scargle periodogram analysis of the total flux density observations, but found no strong evidence for periodicity in any of the sample sources. The only well-established case in support of both jet precession and periodic variability remains the non-sample member OJ 287.

Subject headings: extragalactic objects: general — galaxies: active — polarization — quasars: general — shock waves

1. Introduction

In August 1984 we initiated a program to systematically monitor the sources in the flux and position-limited Pearson-Readhead (Pearson and Readhead 1981, 1988) VLBI survey at cm wavelengths using the University of Michigan 26-meter paraboloid operating at 14.5, 8.0, and 4.8 GHz, with the primary goal of delineating the range of behavior in the total flux and linear polarization in a complete flux-limited sample of extragalactic objects. The source group includes representatives of the optical classes QSO, galaxy, and BL Lac object, as well as of several VLBI morphological classes, making it ideally suited for exploring variability properties as a function of source type. The limit on source flux density provided by the

defining criteria for the sample ($S \geq 1.3$ Jy at 5 GHz) ensured that our observations would provide high signal-to-noise polarization measurements for most sources, since the linearly polarized flux from extragalactic objects is typically on the order of a few percent (Aller, Aller, and Hughes 1996).

Results based on data obtained through 1991.0, and including some heterogeneous earlier measurements for well-known variable sources, were presented in Aller, Aller, and Hughes (1992) (hereafter Paper I), which discussed the statistics of the flux variability and polarization and related them to optical classification and to VLBI morphological classification taken from the literature. The VLBI data then available for comparison were primarily at 5 GHz and lower frequencies. Paper I demonstrated that the QSO group was comprised of both flat and steep spectrum objects with a skew towards flat spectra and that most QSO members were variable, with higher amplitude variations present at 14.5 GHz than at 4.8 GHz, while the galaxies in general exhibited steep spectra, lower-amplitude-to-no flux variability, and longer-term stability in the orientation of the electric vector of the polarized emission (EVPA). This was attributed to the fact that the major contributor to the galaxies' integrated radio emission in most sources was dominated by a contribution from the underlying extended structure rather than from evolving, compact, core (and jet) components.

In the current paper we reexamine those source properties which can be investigated through multifrequency single-dish monitoring data which more than double the time base of Paper I. Our measurements are now supplemented by a wealth of published complementary radio interferometric data at both centimeter and millimeter wavelengths, which has become available through large survey studies undertaken with the VLBA. These include multi-epoch total intensity images matching our own spectral band (Kellermann et al. 1998), as well as total intensity and polarization imaging at a higher frequency, 43 GHz, (Lister 2001a; Jorstad et al. 2001) probing deeper into the inner jet regions. In combination, the single-dish and imaging data provide additional insights into the emission properties of extragalactic objects.

2. OBSERVATIONS

2.1. The Sample

The Pearson-Readhead sample (Pearson and Readhead 1988) (hereafter PR) uses the following selection criteria: 1) declination (1950) $\delta > 35^\circ$; 2) galactic latitude $|b| > 10^\circ$; and 3) total flux density $S \geq 1.3$ Jy based on the NRAO-MPIfR 6 cm strong source surveys. Of the sixty-five sources in the sample, sixty-two are within the declination limit, $\delta < 82^\circ$,

of the University of Michigan 26-m paraboloid. These sources have been systematically observed once every three months at 14.5, 8.0 and 14.5 GHz since fall 1984, following the observing technique and reduction procedures described in Aller et al. (1985) and Aller et al. (2003), with scaling to conform to the flux calibration system of Ott et al. (1994). In addition to the trimonthly observations, sources identified as exhibiting high degrees of activity were incorporated into our core program for more frequent (approximately weekly) observation. Three objects, DA 55, 1928+738, and BL Lac, are also part of a VLBA study we are undertaking to follow the structural evolution at centimeter and millimeter wavelengths in highly active objects (Aller et al. 2001), and hence the data sampling for these sources during the past few years is particularly frequent.

2.2. Emission Properties

The program sources and emission parameters are given in Table 1. These include optical ID, redshift, the radio class based on morphology, both a variability index and a fluctuation index which are discussed below, and the spectral index between 14.5 and 4.8 GHz.

The optical class listed in column 3 for each object is taken from the literature; the sample contains 29 QSOs (Q), 25 galaxies (G), and 8 BL Lac objects (BL). Of the 8 BL Lacs, 6 were also included in the UMRAO flux-limited BL Lac sample (Aller et al. 1999); the remaining two objects, 0814+425 and 1823+568, did not meet the inclusion criteria for the BL Lac sample and are not listed in Burbidge and Hewitt (1987), but are included in the broader compilation given in Burbidge and Hewitt (1992). We note that the optical classifications for three objects have been revised since Paper I as follows: 0212+735 (BL to Q), 3C 371 (G to BL) and OW 637 (G to Q). For 0710+437 we have retained the class G, given in O'Dea (1998) and Peck and Taylor (2000), which differs from the class given in NED.

A diversity of VLBI morphological type, as shown in column 4, is also represented by the member sources. These include compact (c), lobe-dominated (ld), asymmetric (a1 and a2), irregular (i), steep spectrum compact (ssc), following the classification scheme of Pearson and Readhead (1988), and compact symmetric (cso). By radio morphology five steep spectrum compact (ssc) objects and seven confirmed or suspected compact symmetric objects (cso), members of the COINS sample (Peck and Taylor 2000) (identified or candidate compact symmetric objects in the northern sky) are included. A subset of five of these COINS objects (0108+388, 0710+439, 1031+567, 1358+624, & 2352+495) are members of the Stangellini et al. (1998) 1 Jy sample of GHz-peaked-spectrum sources (hereafter GPS),

a group characterized by convex radio spectra with observed turnovers (uncorrected for redshift) near 1 GHz. The centimeter-band spectra of the GHz-peaked sources are typically steep in the high frequency, presumably transparent, part of the spectrum, and past work has characterized them as exhibiting low degrees of variability and low fractional linear polarization (Stangellini et al. 1998). These objects are particularly intriguing because they are postulated to be young on the basis of their small intrinsic sizes, although it has been alternatively proposed that they are small due to confinement by an ambient medium (O'Dea 1998). Four of these GPS sources have been monitored with the VLBA at 15 and 43 GHz to determine motions and inferred kinematical ages (Taylor et al. 2000), yielding ages of 300-1200 years for the current radio activity. Column 5 lists redshifts predominantly taken from NED and from the latest version of the Veron & Veron catalogue available on the web (<http://www.obs-hp.fr/>). Column 6 gives the same variability index, V, used in Paper I at 14.5 GHz and defined to be:

$$V = \frac{(S_{max} - \sigma_{Smax}) - (S_{min} + \sigma_{Smin})}{(S_{max} - \sigma_{Smax}) + (S_{min} + \sigma_{Smin})} \quad (1)$$

This variability index is a measure of the peak-to-trough amplitude change in the total flux during the time window of the observation. In computing parameters characterizing source emission, observations with $\sigma_S > \max(0.1\text{Jy}, 0.03S)$ were excluded to remove observations with unusually poor signal-to-noise. Additionally, some measurements were rejected because of source proximity to the sun. At 14.5 GHz the number of accepted daily averages searched to identify the minimum and maximum fluxes ranged from 53 to 766, with a median value of 85.

While V is an appropriate measure of the flux amplitude change in variable sources, it may not be a useful measure of variability in sources with low-amplitude variability ($V \leq 0.2$) where the variations approach the signal-to-noise level of the measurements. Such values are rare at 14.5 GHz, but are more common at 4.8 GHz where the amplitude of the variability is generally reduced. (See Paper I, Table 1). Also, other investigations have used a measure related to the standard deviation of the data, especially when attempting to identify low-level variability. Therefore, in columns 7 and 8 we include a second variability measure, a fluctuation index which measures the spread about the mean flux and defined as:

$$FI = \left(\left(\frac{\sum X_i^2 \omega_i - \bar{X} \sum X_i \omega_i}{N - 1} - 1 \right) \cdot \frac{N}{\sum \omega_i} \right)^{0.5} \cdot \frac{1}{\bar{X}} \quad (2)$$

Here N is the number of observations of the variable X_i with measurement uncertainty σ_i and weight $\omega_i = \sigma_i^{-2}$. Note that this index attempts to remove the scatter due to measurement errors: an infinite number of measurements of a source where all the scatter is due to normally

distributed measurement errors would yield an expected value of zero. In Figure 1 we show a plot of V versus FI, illustrating that these two indices are highly correlated and showing that V is a reliable measure of variability, permitting comparison of the new variability results with those of Paper I.

Column 9 lists average spectral indices using data at 14.5 and 4.8 GHz. These were computed from paired values of monthly averages; this procedure ensured a time match between the two frequencies for the most poorly observed sources. We adopt the sign convention that $S \propto \nu^{+\alpha}$. Column 10 indicates sources included in higher-frequency VLBI surveys: Lister (2001a); Jorstad et al. (2001); Kellermann et al. (1998) coded L, J, and K respectively. Information on sources which were added to the NRAO 2 cm survey subsequent to Kellermann et al. (1998), and which are available on the World Wide Web via the NRAO URL, are also included.

3. TOTAL FLUX DENSITY VARIABILITY

3.1. Variability Amplitude as a Function of Optical Class and Redshift

Compared to our results on variability from Paper I, the most striking differences using the extended time base occur for galaxies: while 11 sources previously showed no statistically significant variation at 14.5 GHz, several of these now show variability, as shown in Figure 2 and discussed below. In contrast to the outbursts seen in AGNs, the behavior of the variability in the galaxies is characterized by slow changes, either longterm events (e.g., 3C 84 which has shown a single rise and fall extending over nearly four decades), slow, nearly monotonic changes, or infrequent, discrete events (e.g. 3C 390.3: Figure 11). These behaviors are described in detail in section 3.4.

The types of objects showing the largest amplitude variations are BL Lacs and QSOs. A KS test of the distribution of variability index V for the BL Lac objects and for the QSOs gives a probability of 59% that these distributions are drawn from the same population. However, even among the small number of BL Lacs in the sample, there are differences in the details of the variability. These range from large amplitude variations in 0954+658 to lower-amplitude fluctuations in Mkn 501; in the latter a structure function analysis of our early data (Hughes, Aller, and Aller 1992) identified that white noise, rather than shot noise typical of AGNs, characterized the emission process (see also section 4.5).

A relation between variability and redshift might be expected. Therefore, in Figure 2 we plot the fluctuation index at 14.5 GHz versus redshift as a function of optical class. While the redshifts for the galaxies (and BL Lacs) fall in a narrower range ($z < 1.0$) than for the

QSOs, we find no obvious relation between FI and redshift for the sample as a whole. That the amplitude ranges are the same for the BL Lacs and QSOs is clearly evident in this figure.

3.2. Time-Averaged Total Flux Spectrum; Relation to Optical Class and Radio Morphology

Radio spectral index is used as a class delineator in the analysis that follows. To assess whether there are changes in the time-averaged spectra depending on the duration of the time window, we have compared the average spectral indices shown in Table 1 with those determined using data from the first half of the time window only. We find no difference in average α within the standard deviation for each source, and conclude that our average spectral indices appropriately represent the centimeter-band spectra.

Among the sources classed as galaxies, we find only one flat spectrum ($|\alpha| \leq 0.5$) object, 3C 84, a well-known variable source which has exhibited large-amplitude, slow, total flux variations. The remainder of the galaxies have steep spectra ($|\alpha| > 0.5$). In spite of steep total flux spectra, we find that nine of the twenty-five steep-spectrum galaxies vary in flux density at 14.5 GHz with $\text{FI} \geq 0.08$ and $\text{V} \geq 0.17$.

The majority of QSOs have flat spectra, and are variable. However, seven of the twenty-nine QSOs do have steep spectra: 0153+744, 0538+498 (3C 147), 0711+356, 0809+483 (3C 196), 1458+718 (3C 309.1), 1634+628 (3C 343), and 1828+487 (3C 380). By radio morphology, this group includes two compact doubles, four steep spectrum compact objects, and one lobe-dominated source. All of the BL Lacs have flat time-averaged spectra.

As illustrated in Figure 3, at 14.5 GHz most steep spectrum and some flat spectrum objects are found to be variable, while at 4.8 GHz there is a sharp demarcation between the fluctuation indices for these two groups. The distribution of fluctuation index with alpha may be explained in the context of unification schemes invoking orientation-dependent beaming effects. The curves shown superimposed on the 14.5 GHz data in Figure 3 result from computations of a two-component model: an extended, non-variable (presumably unbeam) component with a spectral index of -1.0, and a time variable compact core with a spectral index of 0.5. The locus arises from varying the ratio of the flux density of the core and extended component (as would be expected if a beamed core were observed over a range of viewing angles). The solid curve shows the locus for a core of fixed fluctuation index of 0.5, and the dashed curve shows the case where the core's fluctuation index increases as the observed core flux increases. Such a boost in fluctuation index would result, for example, if the peak flux were preferentially boosted relative to the minimum 'quiescent' flux for cores

seen with the flow axis close to the line of sight, but would be little boosted for edge-on flows. Such a scenario would apply if flow speed is higher during outbursts, or if outbursts reflect distinct emission regions boosted by an additional power of the Doppler factor: in the absence of a particular model, we adopt a linear relation between fluctuation index and core flux as an example of possible behavior. Even a simple proportionality of the fluctuation index to the Doppler boost factor in the modeling gives a clearly better fit to the observed distribution. The low level variability in galaxies probably occurs because in a flux-limited sample they were preferentially selected by their strong extended components rather than by active cores beamed toward us.

3.3. Effects of Bias on Sample Selection

The effects of beaming and redshift on duty cycle, and hence on source selection, have been investigated by Lister (2001b) for flat-spectrum AGNs; he concludes that variability will generally be unimportant in the selection statistics, at least for sources whose flux amplitudes place them well above the threshold value. We concur with Lister (2001b) that this sample is relatively free of bias in source selection, and we believe that it is an appropriate representation of extragalactic objects for statistical study. We note, however, that the full PR sample does, in fact, contain non-blazar-like but variable objects, in addition to presumably highly beamed sources exhibiting blazar-like variability. Additionally, several sources *do* have fluxes near the survey limit; as shown in Figure 4, the time-averaged flux at 4.8 GHz for 1/4 of the sources lies at or below the flux limit for sample inclusion during the period of our study, and one-third of the sample objects decreased in flux to amplitudes below the flux cutoff for durations of one to several years: 0711+356, has remained below the original 5 GHz limiting flux during the entire duration of our study. The possible influences of these factors have not been explored quantitatively.

3.4. Spectral Evolution and Variability Changes

While statistically the values of the time-averaged spectral indices used to separate the flat and steep spectrum objects have not changed on time scales of several years, we identify significant changes in the variability properties of several individual objects. We present and discuss below the light curves for selected objects to illustrate the range of variability we identify. Monthly averages of the UMRAO flux and polarization for all sample members will be included in Aller et al. (2003). We show as examples:

3.4.1. *a flat-spectrum QSO*

In Figure 5 we show the flux and polarization light curves for the QSO 1637+574. The behavior is typical of our program AGNs with large amplitude changes ($V(14.5)=0.54$) and a flat to inverted spectrum ($\alpha_{av} = 0.16$). The April 1999 43 GHz VLBA map of Lister (2001a) shows the source to consist of a core and two jet components with a ‘bend-and-realign’ morphology attributed to flow along a helical path. A large event in the mid-1990s is the dominant feature in the total flux density light curve. Note that the solid line in the lower panel marks the 5 GHz total flux limit for inclusion in the sample. During the 2 year period 1997-1999, and for shorter earlier periods, the total flux at 4.8 GHz was below the flux criterion for sample inclusion.

3.4.2. *an ssc QSO with a masked variable core component*

In Figure 6 we show yearly averages of our longterm data for the QSO 3C 147 which is a prototypical steep spectrum compact source and a ‘typical’ quiescent source proposed as a secondary flux standard (Baars et al. 1977; Ott et al. 1994). Lister’s VLBA map (Lister 2001a) shows a core and some amorphous extended structure at 43 GHz, but no well-defined jet components and a total image size of 4 mas. At 5 GHz, VLBI imaging reveals a jet extending 200 mas to the southwest. The UMRAO integrated total flux data show a steep (transparent) total flux spectrum ($\alpha_{av} = -0.98$) as expected. However, while there are no dominant outburst-like events in the total flux light curve, small systematic changes in the flux are evident on a timescale of several years. These are more evident in Figure 7 which displays yearly averages of the total flux density, with a flux corresponding to the spectrum given by Ott et al. (1994) subtracted from each measured UMRAO datum. Removing this assumed constant component, based on observations obtained during 1989-1992, leaves a clearly identifiable variable component, illustrating that this is a case where the variability of the source is masked by the dominant contribution from extended structure. The fact that the source is variable can be seen directly in the integrated polarization (middle and top panels of Figure 6). Note that the polarized flux shows an inverted spectrum: the source is measurably but only weakly polarized at 4.8 GHz but exhibits stronger polarized flux at 14.5 GHz, at a level comparable to that typical of AGNs (Aller et al. 1999). The EVPAs show a pronounced frequency-dependent separation consistent with, but not totally explained by, an average local rotation measure of -1300 rad m^{-2} reported for the core (Nan et al. 2000). (Complex polarization structure has been identified from VLA mapping (Junor et al. 1999), so we would not expect an unambiguous signature of Faraday rotation in our data.) Based on our data we cannot assess the competing importance of synchrotron

self-absorption and Faraday depolarization near the core.

3.4.3. an ssc QSO exhibiting resolved variability

Figure 8 shows the total flux density and polarization light curves for a second ssc source, QSO 3C 309.1. Unlike the behavior seen in 3C 147, the EVPAs do not show a frequency-dependent offset; and rotation measure mapping has revealed typical rotation measures of only 60 rad m^{-2} , with smaller values in the lobe (Aaron, Wardle, and Roberts 1998). Thus, the physical conditions are different for the two sources in spite of their belonging to the same optical and radio types. Prior to 1992, the total flux light curve is similar to that for 3C 147, exhibiting only low level variations. However, subsequently there is a remarkable change characterized by a large total flux density increase at both 8 and 14.5 GHz, and a corresponding change in spectral index. Significant changes both in the centimeter-band spectrum and in the amplitude of the variability can occur with time scales of order a decade in members of this radio class.

A similar, but less dramatic flux event than that shown in Figure 8 has been seen in a third ssc source in the sample: 3C 380. While it might be expected that ssc sources would not exhibit blazar-like activity, it has been proposed that there are in fact two classes of ssc QSOs, those with prominent cores and superluminal behavior such as 3C 380, 3C 147, and 3C 390.1, and those with weak cores (Akujor 1992). Our data show evidence for blazar-like activity in both 3C 380 and 3C 390.1 which must be associated with changes in evolving components and which would have been missed by a shorter time window because of the length of the times between quiescent and active periods. Indeed, our impression of the variability in 3C 390.1 based on data through 1991.0 was very different from that including the later data. A fourth object from our group with steep centimeter-band spectra, the compact double QSO 0153+744, shows a longterm monotonic decrease in total flux at both 4.8 and 14.5 GHz.

3.4.4. a cso object exhibiting low amplitude flux variability typical of the class

In Figure 9 we show yearly averages of the UMRAO data for the galaxy 0108+388, classed as compact symmetric based on its radio morphology and believed to be one of the youngest members of this class based on its kinematical age of 367 years (Polatidis, Conway, and Owsianik 2002). Because the polarized flux is weak, several EVPAs have not met our acceptance criteria ($P/\sigma_P > 2$) for plotting, and hence are not shown. The source is a

member of the Stangellini 1 Jy GHz-peaked source sample, and we find that it exhibits both low degrees of total flux variability ($FI(14.5)=0.09$), and a low degree of average fractional polarization at 5 GHz ($P_{av} = 0.30 \pm 0.07\%$), as expected for GPS class members. High resolution VLBI images document that the structure of this source is complex, and 15 GHz VLBA observations of total intensity have been modeled assuming 7 components, with the largest fraction of the flux contained in the outermost components on either side of the core, and a relatively low flux contained in the central component identified as the core and center of activity (Taylor, Readhead, and Pearson 1996). The very low level flux variability seen in the bottom panel is typical of csos. Our longterm data support the proposal by Fassnacht and Taylor (2001) that objects of this class be used as VLA calibrators because of the relative stability of their flux levels.

3.4.5. a possibly misidentified cso: variable!

In Figure 10 we show the data for a tentatively identified compact symmetric object (cso) 2021+614 (OW 637). While exhibiting unusual spectral behavior with a turnover at 8.4 GHz, the source is not included in the 1 Jy GPS survey (Stangellini et al. 1998), nor included in O’Dea’s comprehensive list of css and GPS sources (O’Dea 1998). The series of maps from 1994 through 2001 for this source, obtained as part of the 2cm VLBA survey, show the source to be double-sided (Kellermann et al. 1998), as does the 43 GHz map of Lister (2001a). Our light curves show a time-variable spectrum, significant variability at 14.5 and 8 GHz, and a longterm rise at 4.8 GHz. The low degrees of polarization we find are typical of those for GPS sources, but the character of the spectrum and the flux variability are time dependent, very different from those found for 0108+388, and not characteristic of a GPS source. The variability at 14.5 GHz is, in fact, similar to that seen in our program blazars. Lister finds only upper limits on the fractional polarization for the components he has identified at 43 GHz, a result consistent with the low fractional polarization which we find in the centimeter band. A subluminal pattern speed of $0.12 \pm 0.02 h^{-1}c$ has been determined by Tschager et al. (2000). On the basis of the amplitude and timescale of the variations we find, we would have expected superluminal motion.

3.4.6. an ld (lobe-dominated) galaxy with a variable component

Figure 11 shows the flux and polarization for the X-ray bright, lobe-dominated, FR II radio galaxy 1845+797 (3C 390.3). Our data through 1991.0 included in the analysis for Paper I showed some evidence of flux variability, but the data were undersampled for

following these variations in detail. The sampling was subsequently increased at 14.5 GHz, and these data reveal a well-defined, monotonic swing in EVPA at 14.5 GHz during very late 1994-early 1995 associated with the total and polarized flux event which occurred during this period. This result is consistent with the VLBI results of Preuss, Alef, and Kellermann (1996) who find a strong jet feature in their 1995.29 map at 5 GHz which was much weaker in a 1989 image.

3.5. Summary of Variability Properties

We conclude that variability is not restricted to flat spectrum sources and that its characteristic behavior in an individual source can change on time scales of order a decade. Such changes in behavior have previously been identified in UMRAO observations of a few non-sample members, e.g. 3C 120, and OJ 287 (Aller, Aller, and Hughes 1996), both flat spectrum, core-dominated AGNs. Multi-epoch VLBI observations demonstrate that changes in these objects are consistent with the development and evolution of hotspots in the flows of QSO and BL Lac jets. Variability in galaxies is most often not outburst-like, as is commonly found in BL Lacs and QSOs, but rather consists of slower variations, often only identifiable with a time window of order a few decades, or infrequent events, also requiring a long time window to detect variations in the integrated total flux data. We attribute the behavior we see in galaxies to relatively long timescales combined with the low luminosity of the active core components relative to that from the extended structure, requiring an unusually bright event for detection.

4. LINEAR POLARIZATION

Long term linear polarization observations provide information on the characteristics of the quiescent flow - namely the degree of turbulence and the dominant orientation of the magnetic field in the radio-emitting region since, in the optically thin case, the magnetic field orientation is orthogonal to the directly-measured EVPA. Detailed modeling of selected time segments of our multifrequency total flux density and linear polarization observations in three sources exhibiting the expected signature of a propagating shock has provided strong evidence for the passage of a transverse shock in these selected cases (Hughes, Aller, and Aller 1991). In other objects, comparison of changes in the EVPA during active phases and the VLBI parsec-scale structural axis, a measure of the flow direction in the jet, has demonstrated that shocks are most often at oblique angles to the flow direction rather than transverse to it. Such comparisons have used both integrated polarization observations,

when a single component is dominant, (Aller, Hughes, & Aller 1998) and VLBI polarization imaging (Aller et al. 2000; Lister 2001a; Aller, Aller, & Hughes 2002) in cases of complex, as well as simple, structure.

Table 2 contains values of the preferred orientation of the electric vector of the polarized emission and the flow direction indicated by VLBI morphology. Columns 2 and 3 give the adopted rotation measure taken from the literature and its reference. Note that in some well-studied AGNs (of which a few are included here), the central regions have been found to have very large rotation measures which differ from the relatively low rotation measures in other parts of the radio source (Taylor 2000), and which are quite different from the integrated values adopted here. In columns 4 and 5 we give the value of the average percentage polarization at 14.5 GHz computed using the Stokes parameters for the daily observations, and the associated rms scatter (a combination of the measurement error and the variability of the source); these tabulated polarizations have been corrected to avoid systematic bias when polarization measurements with different signal-to-noise ratios are combined (Wardle and Kronberg 1974). The EVPAs in columns 6 and 8 were obtained following the procedure described in detail in Aller et al. (1999). For each source and frequency, a histogram of EVPA was constructed based on monthly averages of the Stokes parameters after correcting for Faraday rotation, using the rotation measures given in column 2. Using a chi-squared test, statistically significant peaks in each distribution were identified which met the acceptance criterion of $\chi^2/N \geq 3$; the fraction of time that the preferred orientation was maintained was also computed. These fractional times are shown in columns 7 and 9. In columns 10-15 we tabulate information on the VLBI parsec scale source orientations compiled from the literature at both centimeter and millimeter wavelengths, and including values of θ measured by us from published maps when no values were cited. The suffixes u, b, and c denote unresolved structure, small scale bends, and largescale curvature respectively, based on our impression of the source structure in the VLBI maps. It is well-documented that there are commonly significant single, or multiple, bends in the jets of AGNs, and in values measured by us we have weighted the dominant parsec scale flow direction $\theta_{5,15,43GHz}$ towards the innermost, best-defined components, or selected from the literature the values based on the inner structure. While maps are available for the compact symmetric objects, their morphology is unusually complex, in several cases exhibiting an ‘S’ symmetry, possibly due to precession of the central engine (Taylor, Readhead, and Pearson 1996), and hence there is not a single, well-defined parsec scale flow direction for these sources. Except for 0404+768, our data show no preferred EVPA at either 4.8 or at 14.5 GHz for members of this group.

4.1. Range of Linear Polarization as a Function of Radio Class

We have examined the average fractional polarization as a function of radio and optical class. We show in Figure 12 the distributions for the compact symmetric (cso) and lobe-dominated (ld) objects at 14.5 and 4.8 GHz. These groups are comprised almost exclusively of galaxies, and, with the exception of 0723+679, they have steep total flux density spectra. For comparison, the distributions are shown for the flat spectrum QSOs and BL Lacs in Figure 13. The number of BL Lacs is small in the sample, but a distribution based on a larger flux-limited sample of BL Lacs can be found in Aller et al. (1999). We note that the QSO 0723+679 is included in both sets of distributions since its properties place it in both categories: it is classed as an ld object based on its radio morphology while we find that the spectral index is flat in the centimeter band. The csos are well-known to have very low degrees of polarization at 4.8 GHz (Stangellini et al. 1998), and this result, combined with recent VLBA observations identifying low values of the polarization at 8.4 GHz, have been used to argue that these objects are depolarized by Faraday rotation in a circumnuclear torus (Peck and Taylor 2000). This interpretation is consistent with the wavelength-dependent fractional polarizations that we find.

In Table 3 we summarize our results on polarization for the lobe-dominated objects in this sample. The detailed polarization structure and spectral variations within the lobes and central regions have been studied with observations from the VLA and sophisticated analysis tools (Katz-Stone et al. 1999). In the case of the FR Is, such data have revealed sheath-like polarization structure in some objects (Hardcastle et al. 1996) and complicated spectral gradients in FR IIs (Treichel et al. 2001). However, our integrated measurements can be used to identify class differences. We list optical class in column 2, and average fractional polarization corrected for bias at 4.8 and 14.5 GHz in columns 3 and 4 respectively. An indicator of the spectrum of the polarized flux (note that this is not fractional polarization) is given in column 5: these are denoted by flat, inverted, or steep (F, I, S), based on visual inspection of the longterm light curves. In some cases the spectrum has changed with time; in these cases (e.g. 0605+480) we list two classes, with the first denoting the most characteristic spectral behavior during the full time window of the study. FR class is listed in column 6. For the FR II class objects we list in column 7 the projected linear size taken from the compilation of Nilsson (1998) which assumes $H=50 \text{ km sec}^{-1}\text{Mpc}^{-1}$ and $q_0=0.5$. For the FR Is we give projected length of the brighter jet originally tabulated in Bridle and Perley (1984) but modified to a value of $H=50 \text{ km sec}^{-1}\text{Mpc}^{-1}$ by Hardcastle et al. (1996) and assuming $q_0=0.5$.

In the three FR Is in the PR sample the spectra of the polarized flux are steep. In the case of the FR IIs we find a range of behaviors: half of the sources have flat-to-inverted

polarization spectra based on the integrated measurements, while the remaining half have steep polarization spectra. We have tried without success to identify a common property from our own and published data, for example source length, which could explain this dichotomy in spectral behavior among a single class. Detailed rotation measure maps and results using spectral tomography have only recently become available for some member sources. In the case of 3C 295 (1409+524), a source characteristically exhibiting an inverted polarization spectrum, a VLA study (Perley and Taylor 1991) plausibly attributed the observed behavior to an intervening screen: Faraday depolarization produced in thermal gas surrounding the source. However, it is not clear whether this explanation can explain the range of behavior in other sources in our study and the temporal variations we find.

4.2. Preferred EVPA

Inspection of the information on EVPA given in Table 2 shows that longterm stability ($\geq 75\%$ of the time) at 4.8 GHz was found in 28 of the 62 sources, of which 12 are galaxies. In contrast, at 14.5 GHz only 7 sources show a statistically significant preferred EVPA $\geq 75\%$ of the time; however, several sources show preferred EVPAs for more than a third of the time. Of these 7 objects with longterm, stable EVPAs, 5 are variable QSOs, one is a variable BL Lac and only one is a steep-spectrum, quiescent, lobe-dominated galaxy. For the highly variable sources, in particular the BL Lacs, we had attributed the lack of long-term preferred EVPA at 14.5 GHz to the fact that the integrated polarization is dominated by contributions from evolving source components near, or in, the core (Aller et al. 1999). However, we find here that even among the BL Lacs, long-term preferred EVPAs do exist over significant portions of the time window, and over time periods which include several events. This suggests that the magnetic field may have a ‘memory’, in the central radio-band regions, and that subsequent outbursts in a source may exhibit the same or a related magnetic field structure, or, alternatively, that there is a persistent standing shock in the ‘core’.

Figure 14, showing the data for QSO 0212+738, illustrates another behavior we find in some AGNs: a preferred EVPA which changes abruptly to a second longterm preferred EVPA. Such behavior has previously been identified in non-sample members 1308+326 (Aller et al. 1999) and 3C 279 (Aller, Aller, and Hughes 1996). In 0212+738 we find a longterm preferred EVPA at 4.8 GHz which is maintained in spite of the nearly continuous activity in the source. The average centimeter-band spectral index is very flat: $\alpha = 0.03$. At 14.5 GHz, however, we find two preferred orientations: a first near to the value preferred at 4.8 GHz until 1995, followed by a rotation, and a second relatively stable orientation nearly

orthogonal to the earlier value. This frequency-dependent EVPA separation has continued to the present time. We attribute this behavior to a change in the opacity in the cm-band emitting region indicated by the evolution of the spectrum of the total flux density: the source has become transparent, so that at 14.5 GHz we are looking further into the jet at a region which has a substantially different magnetic field alignment. The 43 GHz map of Lister (2001a) at epoch 1999.26 shows four jet components, significant polarization from both the core and jet, and a total polarization of 4.9%. While our data represent a sum of contributions from all components and extended structure, the change we see is consistent with increased emission from the strongest VLBI component. Both the millimeter VLBA data and single dish centimeter-band data suggest that at this epoch the predominant magnetic field is aligned nearly perpendicular to the flow direction of $\sim 111^\circ$. The behavior illustrates that significant changes in the characteristic behavior of the polarization, as well as of the flux, can occur with time scales of a decade and that shorter time windows (even a decade long) may not adequately sample the range of variability. In the case of this source, a sequence of well-sampled high frequency VLBP maps would have been helpful in unraveling the complicated behavior we find.

4.3. Relation of Magnetic Field Orientation to Flow Direction: Class-Dependent Differences

In Paper I we compared the preferred intrinsic EVPAs at 14.5 and 4.8 GHz with the flow direction (θ) in the jet indicated by the morphology apparent in the 5 GHz Pearson-Readhead maps (Pearson and Readhead 1988). We found that at 14.5 GHz there was no difference in distribution of $|\text{EVPA}-\theta|$ between QSOs and BL Lacs, but at 4.8 GHz the values of $|\text{EVPA}-\theta|$ clustered near 0-20° for the BL Lacs and were preferentially near 90° for the QSOs; the disparity between the shape of the distribution of orientation difference for each optical class based on our data at 4.8 GHz suggested intrinsic differences in the physical properties of the objects such that the magnetic field in the emitting region is preferentially along the flow direction in QSOs and perpendicular to it in BL Lacs. This result supports the class differences in EVPA orientation identified in Cawthorne et al. (1993), but differs from it in concept since that result is based on single-epoch observations of jet (and core) components with typical lifetimes of order a decade (Gabuzda et al. 1994) while our result is based on longterm data, which may include many different evolving components (which might have exhibited quite different EVPAs from event to event), and with the major contribution to the integrated polarization most likely arising in the core and innermost jet components at 14.5 GHz (Homan et al. 2002).

With the substantial data set and higher resolution VLBI maps now available, we reexamine the question of the class-dependence of the magnetic field orientation. Inspection of Table 2 shows that there is a range of values for the flow direction found from the maps at the various wavelengths for each source, which can be as large as tens of degrees. This may result from curvature in the jet flow combined with scale differences in the regions probed with the different observing frequencies, complicating the selection of the most appropriate value for a comparison between the flow direction and the EVPA. Further, the preferred polarization orientations found at 14.5 and at 4.8 GHz differ by several degrees in some sources. That difference may result from opacity effects within the source so that the integrated emission arises from slightly different regions, with differing magnetic field orientations. Alternatively the frequency-dependent spread in preferred EVPA may indicate that our adopted rotation measure is incorrect in some sources. Rotation measure mapping of several objects, (Taylor 2000; Mutel and Denn 2000; Reynolds et al. 2001), has demonstrated that the rotation measure for the core can be very high and that it can vary significantly from epoch to epoch. We have assumed that the rotation measure is spatially and temporally invariant. All of the above factors combine to complicate a comparison of the magnetic field orientations, deduced from the polarization, with the flow direction in the jet.

In Table 4 we show a grid of values comparing EVPA and θ_ν for the BL Lacs of the sample. Note that there is an ambiguity of 180° in the determination of the EVPAs and that we have restricted the orientation difference to lie within a 90° range. We find that the orientation difference, $|\text{EVPA}-\theta|$, is generally $\leq 36^\circ$ (see discussion of 3C 371 below) confirming the result from Paper I that in BL Lacs the magnetic field orientation (orthogonal to the EVPA) is preferentially aligned transversely to the flow direction. Lister (2001a) has looked at the distribution of the EVPA of the core with respect to the innermost jet direction in BL Lacs using single epoch 43 GHz VLBI observations and also finds that these offsets are confined to the range $\leq 40^\circ$. That these distributions are similar is consistent with Lister’s conclusion that the bulk of the polarized emission on parsec scales in flat spectrum members of the PR sample comes from the core component. This result appears to imply that there is a preferred EVPA of the core component over the longterm, but that this can change with time as unresolved components emerge with different orientations. Earlier results at 5 GHz by Gabuzda and coworkers, e.g., Gabuzda and Cawthorne (1992), also showed systematic differences in the polarization structure in BL Lacs and QSOs, but these were based on the distributions for jet components, and not for the cores, which showed no clear preferred range of orientation.

In Figure 15a we compare the orientation difference between the preferred intrinsic EVPA at 4.8 GHz (χ_0 in Table 3) and the flow direction at the highest VLB frequency (generally 43 GHz, but supplemented by observations at 15 GHz for three galaxies) for all

PR sample sources with both a well-defined flow direction and a preferred EVPA. The objects have been separated by optical class. We chose this frequency because of the larger number of sources which exhibit preferred EVPAs, and for comparison with earlier work based on VLBP observations at this frequency. The distribution is consistent with a systematic difference between the behavior for QSOs and for BL Lacs such that the dominant persistent magnetic field orientation is along the flow direction in QSOs (orientation difference near 90°) and perpendicular to it in BL Lacs. We note that there is a large range of values for the QSOs; for the BL Lacs the values are closely clustered. An exception is the BL Lac object 3C 371 which shows a large orientation difference characteristic of a QSO; however, in this source Lister has found no polarization in the core at 43 GHz, in agreement with the earlier 5 GHz result of Gabuzda et al. (1989), suggesting that our measured polarization originates in extended structure. The suggestion is consistent with the arcsecond scale polarization mapping of the source at 1.4 GHz by Stangellini et al. (1997). A KS test of the distributions for the BL Lacs and QSOs gives a probability of 3.97% that they are drawn from the same parent population. A χ^2 test of the distribution for the QSOs gives a probability of 2.1% that this distribution is random. Thus, our result is suggestive at the 2σ level of two different populations. Within the shock-in-jet scenario this would be consistent with differences in the allowed range of obliquities relative to the flow direction, or alternatively to the increased importance of a longitudinal magnetic field component in QSO flows, possibly related to shear. These alternatives are discussed in section 5.

Because the polarization measurements at 4.8 GHz may contain contributions from unresolved components near the core, we show in Figure 15b the same plot based on the preferred intrinsic EVPAs at 14.5 GHz. We have included all sources for which a significant preferred EVPA was identified; in general these are maintained for shorter time intervals than at 4.8 GHz. All of the BL Lacs in the sample exhibit preferred EVPAs at 14.5 GHz, as well as at 4.8 GHz. However, nine QSOs which exhibited preferred EVPAs at 4.8 GHz do not exhibit them at 14.5 GHz, with the converse for one source: the ssc object 0538+498 which has very weak polarization at 4.8 GHz. Unfortunately, there are only 21 sources with both preferred EVPAs and well-identified flow directions at 14.5 GHz which weakens statistical tests due to small numbers. Nevertheless, while the distribution for the QSOs now more closely resembles a random one, the BL Lacs remain clustered near small orientation differences, with the exception of 3C 371 already discussed.

4.4. Systematic Temporal Changes in EVPA

We have examined the temporal variations in EVPA to look for behavior which might be expected as a signature of a precessing jet, and were unable to identify such behavior. Prime candidates might be the compact symmetric objects, which are believed to be young and possibly precessing based on their unusual VLBI morphologies (Taylor, Readhead, and Pearson 1996); however, as already discussed, the polarization is relatively low in these objects. Furthermore, if geometric precession were to occur in the jets of some sample members, the expected systematic variations in EVPA might be masked by the changes in the evolving source components contributing to our integrated polarization. As an added complication, the expected precession period even in the relatively rapid variable, OJ 287, is estimated to be 130 years (Lehto and Valtonen 1996) and even longer in other objects (Katz 1997), while our observational time window is only of order a few decades. Thus, it is uncertain whether the expected signature could, in practice, be identified.

4.5. Results of Search for Periodicity

We have carried out Scargle periodogram analyses on all sources in the sample and find no *strong* evidence for periodicity in any of the sample sources based on our data. Evidence for quasiperiodicity in the radioband light curves for sample member DA 55, based on a time series analysis, has been carried out by Pyatunina (2002), and both the radio structure and broadband spectral evolution suggest helical jet structure in a second sample source 0954+658 (Raiteri 1999). Past attempts to identify periodicity in the centimeter band emission from UMRAO data alone, in even the most active AGNs, using both Scargle periodograms and Morlet wavelets, have been hampered by the fact that large, discrete events occur typically only once every few years. Hence, while there have been hints of periodicity in the analysis for a few objects exhibiting several events, e.g. Roy et al. (2000), these determinations have not had high significance except in the case of OJ 287 (Hughes, Aller, and Aller 1998) which also remains the best case for precession (Valtaoja et al. 2000). A longer timebase increases the prospects of identifying periodic behavior, if present, in any of these sources.

The Scargle periodogram analysis identifies marginally significant power peaks in four sources (0804+499, 0954+658, 1637+574, & 1739+522), but these may be tied to the window function or be cases of aliasing, and a longer time period of observations will be required for verification. For two of these four objects an independent structure function analysis yielded unusually short characteristic timescales (0.63 years for 1739+522 and 1.1 year for 1637+574) compared to the average value of ~ 2 years found from analysis of a sample of

highly active objects (Hughes, Aller, and Aller 1992) suggesting that further observation of these selected objects is warranted and that they may be special cases exhibiting unusual variability properties. For 0804+499 a structure function analysis identifies wavelength-dependent characteristic timescales and the shortest time scale we have found for any source: 0.15 years at 14.5 GHz. This source is an intraday variable (Wagner and Witzel 1991), but our data probe a different time domain, identifying a time scale of order 2 months. The periodogram analysis also identifies an unusually broad distribution of power in two sources (0016+731 and Mkn 501) relative to the results for other sources and is consistent with white noise structure functions, perhaps resulting from temporally undersampled, very short timescale activity. We conclude that while the search for periodicity was inconclusive, it has identified unique, interesting objects worthy of further investigation. A recently completed cross wavelet analysis of the data is presented in Kelly et al. (2002).

5. DISCUSSION AND CONCLUSIONS

While our light curves have allowed us to delineate the characteristics of the variations in the emission, understanding the evolution of the jet flow, its origin, and its relationship to the putative black hole which fuels it can best be accomplished by a combination of well-sampled light curves and VLBI/P images at several frequencies, with adequate time resolution to follow the evolution of individual features. Such maps are now available for limited time periods for a handful of sources, selectively chosen to be blazar-type AGNs, e.g., Homan et al. (2001, 2002), but, as demonstrated here, such AGNs represent only one facet of the variability phenomenon.

Within the framework of a shocked-jet model, associating the variability we find in both total and polarized flux with the development of shocks in the flow, our results on magnetic field orientation suggest that in BL Lacs shocks develop with a limited range of obliquity to the flow direction and are preferentially nearly transverse to the flow direction; in QSOs the range is larger and preferentially at large angles to it suggesting that oblique shocks, rather than transverse ones, form in these flows. It has been proposed that the longitudinal magnetic field alignment observed in QSOs is due to shear (Cawthorne et al. 1993). However, while shear could produce an increase in polarization associated with the ordering of the field, it would result in a very specific field orientation. Thus we prefer an explanation invoking shocks with a range of obliquities to the flow direction, an explanation which is consistent with the structural evolution seen in time series of VLBA polarization maps. While shear, to some degree, is expected in the flows, either as a vortex sheet at the jet-ambient medium interface, or in a shear layer permeating the emitting region, no

quantitative shear models for parsec-scale jets currently exist for specific tests against the data. Additionally, we do not believe that the observational evidence cited in favor of shear is unambiguous: 1) while VLBP maps of the QSO 1055+018 and of the BL Lac-type object 0820+225 show longitudinal sheath-like magnetic fields in the parsec-scale flows, we do not believe that there is conclusive evidence that these are associated with shear, nor do these two cases explain the QSO-BL Lac dichotomy since one of the objects is a BL Lac; 2) recent analysis of VLBP maps for 12 blazars (Homan et al. 2002) observed during a one-year time period showed that the EVPAs of the jet features rotated with time such that the magnetic field has become more aligned with the jet axis with increasing distance from the core, but the origin of the change in net field orientation could not be unambiguously identified: it is neither clear whether an increased importance of shear with core distance could produce such changes within the linear dimensions probed, nor was the expected associated increased ordering of the field identified in 4 of the 5 cases. Temporal changes in EVPA are currently being studied within the framework of evolving oblique shock models using VLBA data obtained over a 30-month time span, allowing a larger range of core distances to be explored, and including a wider range of frequencies (Aller, Aller, & Hughes 2002).

Precession has been discussed widely in the literature, and might be expected based on the range of morphologies seen in maps from VLB surveys (Kellermann et al. 1998), but we are unable to identify its expected signature in our data. A combination of longterm monitoring data and VLBI mapping may lead to more conclusive evidence, and the data included in a recent study of the BL Lac object ON 231 (Massaro et al. 2001) is an observational initial step in this direction. However, while evidence supporting the helical character of jet flows is strong, this may result from instabilities in the flow rather than from precession (Hardee, Hughes, Rosen, and Gomez 2001). Thus, in our view, a convincing case for precession has only been made for a single source: OJ 287.

The millimeter imaging data now available, combined with sophisticated analysis tools, permit studies of the evolution of the structure in the inner regions of the jet. With the aid of such modeling, it is now possible to follow the structural development of individual regions in both polarization and total flux, and to identify the complex changes in the flow direction, including bends and changes in the underlying magnetic field direction on sub-milliarcsecond scales. These data probe quite different regions from those initially studied at 5 GHz, and both opacity effects and Faraday effects are reduced. Detailed model fitting in the range 15 to 43 GHz has already demonstrated that the so-called ‘core’, may, in fact, contain contributions from newly-emerging, blended components, further complicating an earlier simpler picture. Indeed, recent model fitting of the VLBP data for some core-dominated blazars, of both the BL Lac and QSO classes, demonstrate quantitatively that the major contribution to the integrated polarized flux comes from the ‘core’ itself or the

next innermost component (Gabuzda and Cawthorne 2000; Homan et al. 2002). Clearly, flux and polarization monitoring at well-selected frequencies remains an essential tool for probing the detailed changes in the jet flow and unraveling the complex opacity-dependent effects within it. Hopefully, a combination of imaging and monitoring of both blazars and other types of extragalactic objects will ultimately lead to a more complete understanding of their origin and evolution.

Finally, while we continue to believe that the features of the variability apparent in our data can most readily be explained within the standard picture of relativistic jet flows containing passive magnetic fields and the naturally-developing instabilities within them, we note that an alternative picture has recently been proposed by Blandford (2003) based on dynamo models and ensuing currents. Once detailed predictions of the flux and polarization are available for this class of model, it will be most interesting to compare them with the range of behaviors discussed here.

Our main results are as follows:

1. We identify variability in steep spectrum objects (ssc and cd classes by radio morphology) which is characterized by infrequent events or longterm monotonic changes. This group includes 3C 147 and calls into question its use as a secondary flux standard.
2. We have tentatively identified small-amplitude variations in several lobe-dominated sources including 3C 179, 3C 236, and 3C 390.3. These variations are consistent with information on core strengths and the ratio of core to total flux known from radio maps of those objects.
3. We have provided evidence in support of our view that variability is a pervasive phenomenon in extragalactic objects, and that the majority of extragalactic objects exhibit activity which can be identified from integrated light curves over time periods of order 1-2 decades. This long time range is crucial for the case of the steep spectrum objects where large events are required for detection because of the dominant contribution from extended structure.
4. We find no strong evidence for periodicity for any sample members based on a Scargle periodogram analysis of our total flux density data, nor are we able to identify the signature of precession in the temporal evolution of the EVPAs.
5. We find a range of behavior in the polarization spectra of the steep-spectrum objects. The flat-to-inverted spectra we find in several source members is consistent with Faraday depolarization by a Faraday screen.
6. We find longterm EVPA stability in many objects indicative of a persistent, dominant

magnetic field orientation. When compared with flow directions from VLBI morphology, the field directions are consistent with class-dependent differences between BL Lac and QSO flows.

This work has been supported in part by NSF grants AST-8815678, AST-9120224, AST-9421979, and AST-9900723. We thank A. Polatidis for providing unpublished jet orientations at 6 cm, H. Falcke for useful suggestions regarding the identification of variability in lobe-dominated sources, M. Lister for providing results in advance of publication and for insightful comments, and an anonymous referee for comments which improved the content and presentation of the paper. We gratefully thank J. A. Zensus both for permission to quote results based on unpublished maps from the 2 cm VLBA survey (MOJAVE), and for his hospitality at MPIfR to M.F.A. and H.D.A. where part of this research was carried out. Finally, M.F.A. and H.D.A. thank NRAO for its hospitality during which this work was completed. This research made use of the NASA/IPAC Extragalactic Database (NED) which is operated by the Jet Propulsion Laboratory, California Institute of Technology under contract with NASA. The operation of the 26-meter telescope is supported by the University of Michigan Department of Astronomy.

REFERENCES

Aaron, S. E., Wardle, J. F. C., & Roberts, D. H. 1998, in Radio Emission from Galactic and Extragalactic Compact Sources, ed. J. A. Zensus, G. B. Taylor, & J. M. Wrobel (San Francisco, CA: ASP), 105

Akujor, C. E. 1992, in Variability of Blazars, ed. E. Valtaoja & M. Valtonen (Cambridge U. Press: Cambridge), 251

Aller, H. D., Aller, M. F., & Hughes, P. A. 2002, Proceedings of the 6th European VLBI Network Symposium, ed. E. Ros, R. W. Porcas, & J. A. Zensus, astro-ph 0210636

Aller, H. D., Aller, M. F., Hughes, P. A., Wardle, J. F. C., Homan, D. H., & Roberts, D. H. 2000, BAAS, 32, 1523

Aller, H. D., Aller, M. F., Hughes, P. A., Wardle, J. F. C., Roberts, D. H., & Homan, D. C. 2001, BAAS, 33, 1455

Aller, H. D., Aller, M. F., Latimer, G. E., & Hodge, P. E. 1985, ApJS, 59, 513

Aller, H. D., Aller, M. F., Latimer, G. E., & Hughes, P. A. 2003, in preparation

Aller, H. D., Hughes, P. A., & Aller, M. F. 1998, in IAU Colloquium 164: Radio Emission from Galactic and Extragalactic Compact Sources, ed. J. A. Zensus, G. B. Taylor, & J. M. Wrobel (San Francisco, CA: ASP), 167

Aller, M. F., Aller, H. D., & Hughes, P. A. 1992, ApJ, 399, 16

Aller, M. F., Aller, H. D., & Hughes, P. A. 1996, in Blazar Continuum Variability, ed. H. R. Miller, J. R. Webb, & J. C. Noble (San Francisco, CA: ASP), 193

Aller, M. F., Aller, H. D., Hughes, P. A., & Latimer, G. E. 1999, ApJ, 512, 601

Baars, J. W. M., Genzel, R., Pauliny-Toth, I. I. K., & Witzel, A. 1977, A&A, 61, 99

Blandford, R. 2003, Circular polarisation in relativistic jet sources, ed. R. Fender & J.-P. Macquart, Astrophysics & Space Science, in preparation

Bridle, A. H., & Perley, R. A. 1984, ARA&A, 22, 319

Burbidge, G., & Hewitt, A. 1987, AJ, 93, 1

Burbidge, G., & Hewitt, A. 1992, in Variability of Blazars, ed. E. Valtaoja & M. Valtonen (Cambridge: Cambridge University Press), 4

Cawthorne, T. V., Wardle, J. F. C., Roberts, D. H., & Gabuzda, D. C. 1993, *ApJ*, 416, 519

Fassnacht, C. D., & Taylor, G. B. 2001, *AJ*, 122, 1661

Gabuzda, D. C., & Cawthorne, T. V. 1992, in *Variability of Blazars*, ed. E. Valtaoja & M. Valtonen (Cambridge: Cambridge U. Press), 238

Gabuzda, D. C., Mullan, C. M., Cawthorne, T. W., Wardle, J. F. C., & Roberts, D. H. 1994, *ApJ*, 435, 140

Gabuzda, D. C., & Cawthorne, T. V. 2000, *MNRAS*, 319, 1056

Gabuzda, D. C., Cawthorne, T. V., Roberts, D. H., & Wardle, J. F. C. 1989, *ApJ*, 347, 701

Gabuzda, D. C., Pushkarev, A. B., & Cawthorne, T. V. 2000, *MNRAS*, 319, 1109

Hardcastle M. J., Alexander, P., Pooley, G. G., & Riley, J. M. 1996, *MNRAS*, 278, 273

Hardee, P. E., Hughes, P. A., Rosen, A., & Gomez, E. A. 2001, *ApJ*, 555, 74

Homan, D. C., & Wardle, J. F. C. 1999, *AJ*, 118, 1942

Homan, D. C., Ojha, R., Wardle, J. F. C., Roberts, D. H., Aller, M. F., Aller, H. D., & Hughes, P. A. 2001, *ApJ*, 549, 840

Homan, D. C., Ojha, R., Wardle, J. F. C., Roberts, D. H., Aller, M. F., Aller, H. D., & Hughes, P. A. 2002, *ApJ*, 568, 99

Hughes, P. A., Aller, H. D., & Aller, M. F. 1991, *ApJ*, 396, 469

Hughes, P. A., Aller, H. D., & Aller, M. F. 1992, *ApJ*, 396, 469

Hughes, P. A., Aller, H. D., & Aller, M. F. 1998, *ApJ*, 503, 662

Jorstad, S. G., Marscher, A. P., Mattox, J. R., Wehrle, A. E., Bloom, S. D., & Yurchenko, A. V. 2001, *ApJS*, 134, 181

Junor, W., Salter, C. J., Saikia, F., Mantovani, F., & Peck, A. B. 1999, *MNRAS*, 308, 955

Katz, J. I. 1997, *ApJ*, 478, 527

Katz-Stone, D. M., Rudnick, L., Butenhoff, C., & O'Donoghue, A. A. 1999, *ApJ*, 516, 716

Kellermann, K. I., Vermeulen, R. C., Zensus, J. A., & Cohen, M. H. 1998, *AJ*, 115, 1295

Kelly, B. C., Hughes, P. A., Aller, H. D., & Aller, M. F. 2002, *ApJ*, submitted

Lehto, H. J., & Valtonen, M. J. 1996, *ApJ*, 460, 207

Lister, M. L. 2001a, *ApJ*, 562, 208

Lister, M. L. 2001b, *ApJ*, 561, 676

Marr, J. M., Taylor, G. B., & Crawford, F., III. 2001, *ApJ*, 550, 160

Massaro, E., Mantovani, F., Fanti, R., Nesci, R., Tosti, G., & Venturi, T. 2001, *A&A*, 374, 435

Mutel, R., & Denn, G. 2000, *BAAS*, 32, 1522

Nan, R. D., Zhang, H. Y., Gabuzda, D. C., Ping, J. S., Schilizzi, R. T., Tian, W. W., & Inoue, M. 2000, *A&A*, 357, 891

Nilsson, K. 1998, *A&AS*, 132, 31

O'Dea, C. P. 1998, *PASP*, 110, 493

Ott, M., Witzel, A., Quirrenbach, A., Krichbaum, T. P., Standke, K. J., Schalinski, C. J., & Hummel, C. A. 1994, *A&A*, 284, 331

Pearson, T. J., & Readhead, A. C. S. 1981, *ApJ*, 248, 61

Pearson, T. J., & Readhead, A. C. S. 1988, *ApJ*, 328, 114

Pearson, T. J., & Readhead, A. C. S. 2000, *ApJ*, 541, 112

Peck, A. B., & Taylor, G. B. 2000, *ApJ*, 534, 90

Perley, R. A., & Taylor, G. B. 1991, *AJ*, 101, 1623

Pohl, M., & Schlickeiser, R. 2000, *A&A*, 354, 395

Polatidis, A. G., Conway, J. E., & Owsianik, I. 2002, in *Proceedings of the Sixth European VLBI Network Symposium*, eds. E. Ross, R. W. Porcas, A. P. Lobanov, & J. A. Zensus (Bonn, Germany), 139.

Preuss, E., Alef, W., Kellermann, K. I. 1996, in *Extragalactic Radio Sources*, ed. R. Ekers, C. Fanti, & L. Padrielli (Kluwer: Dordrecht), 34

Pyatunina, T. 2002, Private communication.

Raiteri, C. M., et al. 1999, *A&A*, 352, 19

Reynolds, C., Cawthorne, T. V., & Gabuzda, D. C. 2001, MNRAS, submitted

Roy, M., Papadakis, I. E., Ramos-Colón, E., Sabruna, R., Tsinganos, K., Papamastorakis, J., & Kafatos, M. 2000, ApJ, 545, 758

Rudnick, L., & Jones, T. W. 1983, AJ, 88, 518

Rudnick, L., Zukowski, E., & Kronberg, P. P. 1983, A&AS, 52, 317

Rusk, R. E. 1988, Ph D. Thesis, University of Toronto

Simard-Normandin, M. Kronberg, P. P., & Button, S. 1981, ApJS, 45, 97

Stangellini, C. Dallacasa, D., Bondi, M., & Della Ceca, R. 1997, A&A, 325, 911

Stangellini, C., O'Dea, C. P., Dallacasa, D., Baum, S. A., Fanti, R., & Fanti, C. 1998, A&AS, 131, 303

Taylor, G. B. 2000, ApJ, 533, 95

Taylor, G. B., Marr, J. M., Pearson, T. J., & Readhead, A. C. S. ApJ, 541, 112

Taylor, G. B., Readhead, A. C. S., & Pearson, T. J. 1996, ApJ, 463, 95

Treichel, K., Rudnick, L., Hardcastle, M. J., & Leahy, J. P. 2001, ApJ, 691, 702.

Tschager, W., Schilizzi, R. T., Röttgering, H. J. A., Snellen, I. A. G., & Miley, G. K. 2000, A&A, 360, 887

Valtaoja, E., Teräsranta, H., Tornikoski, M., Sillanpää, A., Aller, M. F., Aller, H. D., & Hughes, P. A. 2000, ApJ, 531, 744

Wagner, S. J., & Witzel, A. 1991, in Extragalactic Radio Sources-From Beams to Jets, ed. J. Roland, H. Sol, & G. Pelletier (Cambridge: Cambridge U. Press), 59

Wardle, J. F. C., & Kronberg, P. P. 1974, ApJ, 194, 429.

Wehrle, A. E., Unwin, S. C., Aller, H. D., Aller, M. F., & Nicolson, G. 1996, in Blazar Continuum Variability, ed. H. R. Miller, J. R. Webb, & J. C. Noble (San Francisco, CA: ASP), 285

Wrobel, J. 1987, in Superluminal Radio Sources, ed. J. A. Zensus, & T. J. Pearson (Cambridge: Cambridge University Press), 186

Wrobel, J. M. 1993, AJ, 106, 444

Xu, C., O'Dea, C. P., & Biretta, J. A., 1999, AJ, 117, 2626

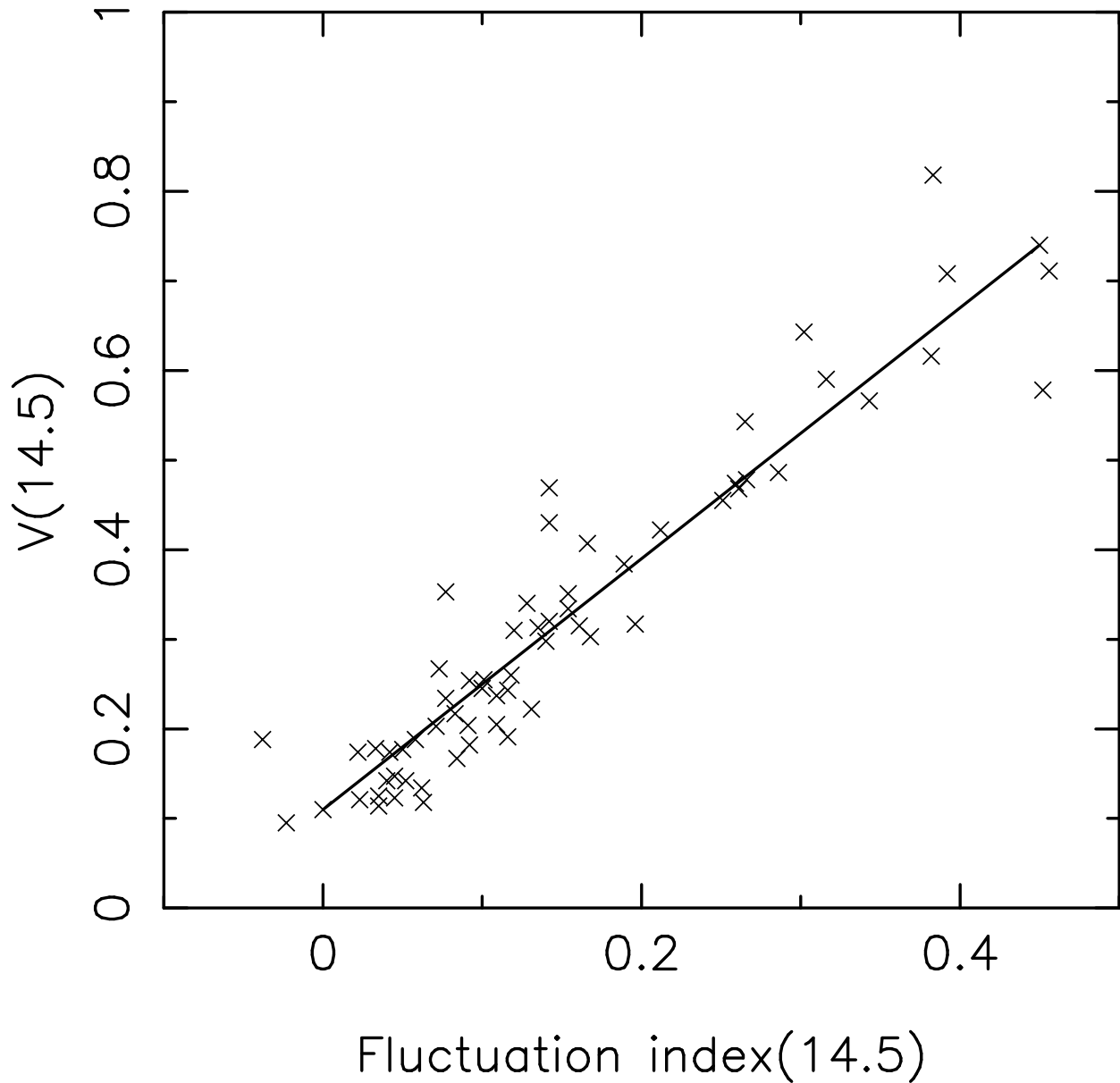


Fig. 1.— Variability index versus fluctuation index based on data during 1984.58-2001.25. The line denotes a least squares fit to the data. The correlation coefficient is 0.937. The source with the unusually high amplitude variability is the BL Lac object 0954+658.

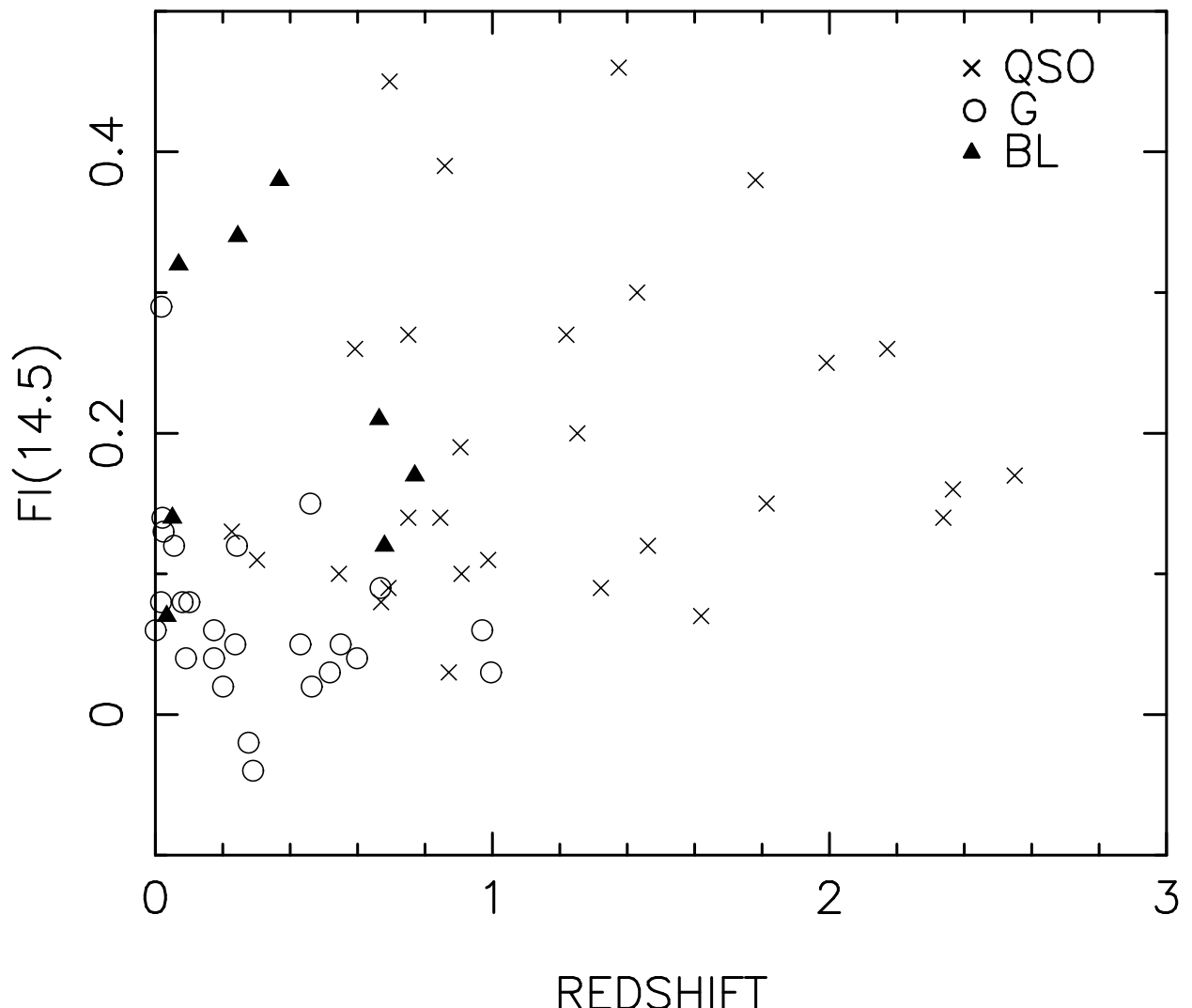


Fig. 2.— Fluctuation index versus redshift. The objects have been coded by optical class. Note that with the exception of 3C 84, the galaxies have $FI(14.5) \leq 0.16$.

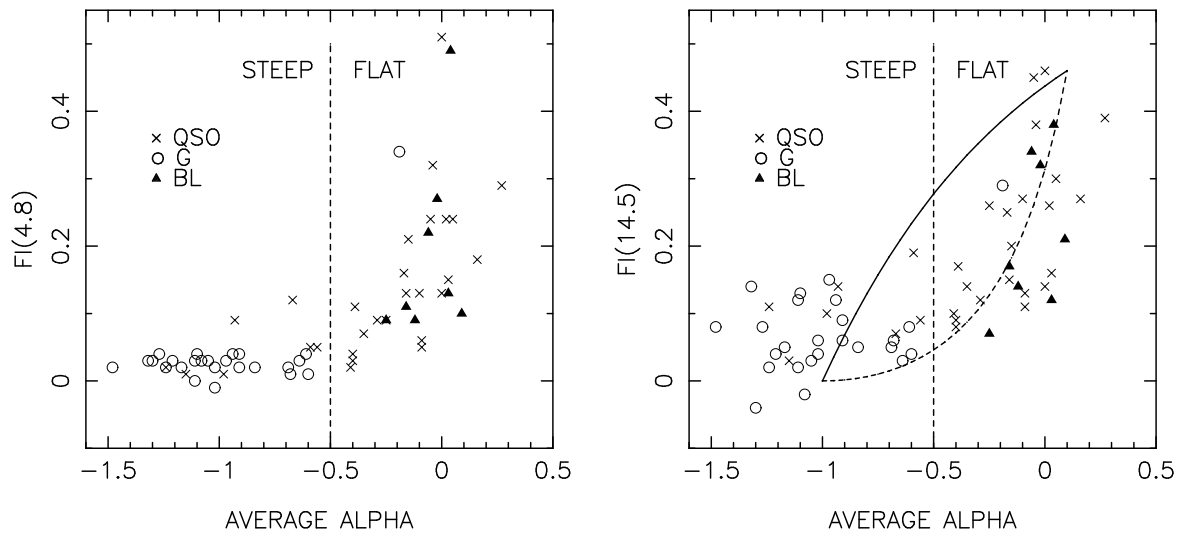


Fig. 3.— Left: fluctuation index at 4.8 GHz versus average alpha (14.5-4.8 GHz) based on data in the time interval of this paper: 1984.58-2001.25. The objects have been coded by optical class, and the demarcation between flat and steep spectrum objects is marked by the dashed vertical line. Right: fluctuation index at 14.5 GHz versus alpha. The full and dashed curves shows the locii for two assumed two-component models as described in the text.

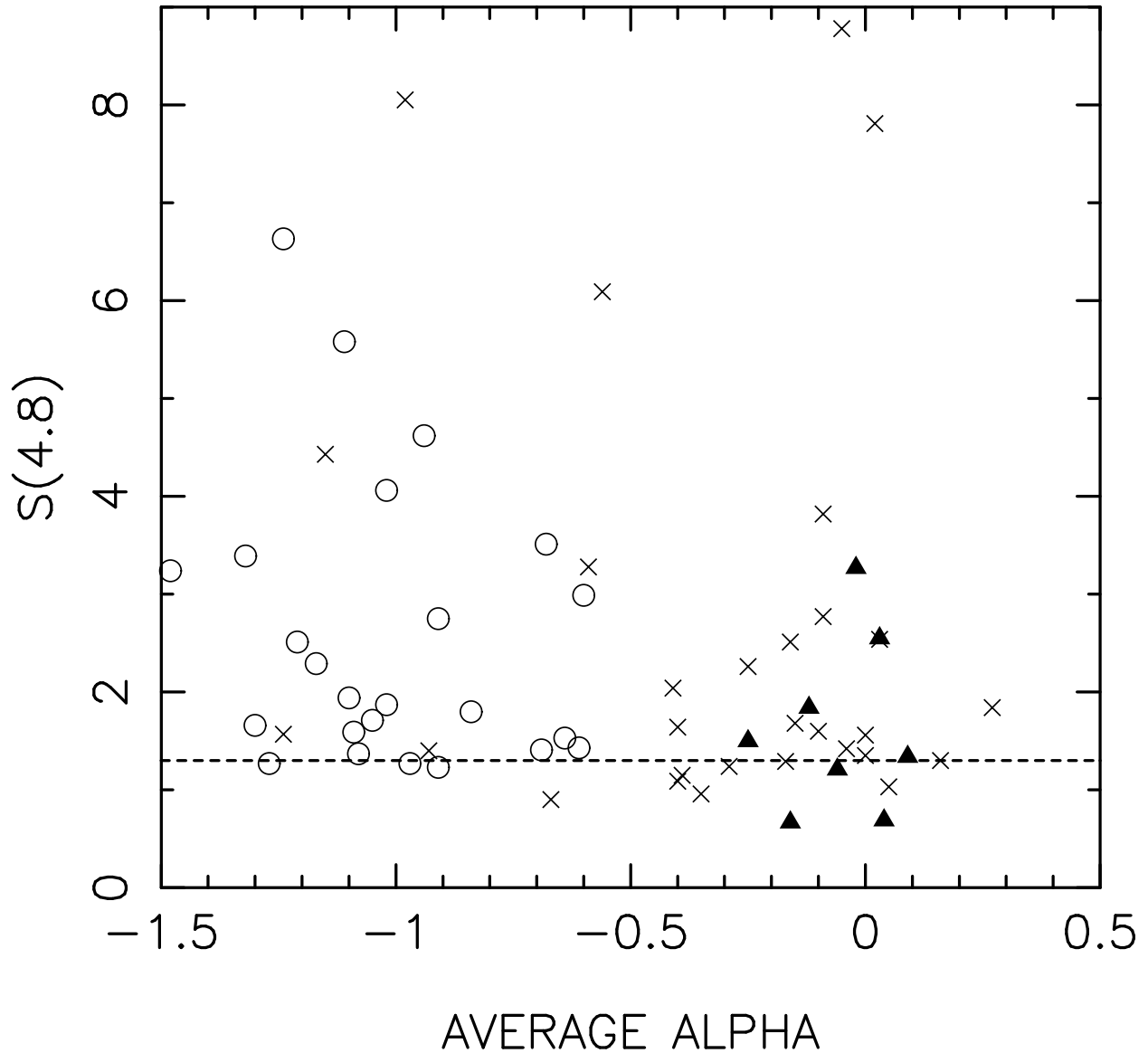


Fig. 4.— Average 4.8 GHz flux versus average spectral index during 1984.58-2001.25. The dotted horizontal line marks 1.3 Jy, the 5 GHz flux density used for source selection. Sources below this line would not have been included in the survey based on their average flux density. The very bright source 3C 84 lies outside the flux range shown.

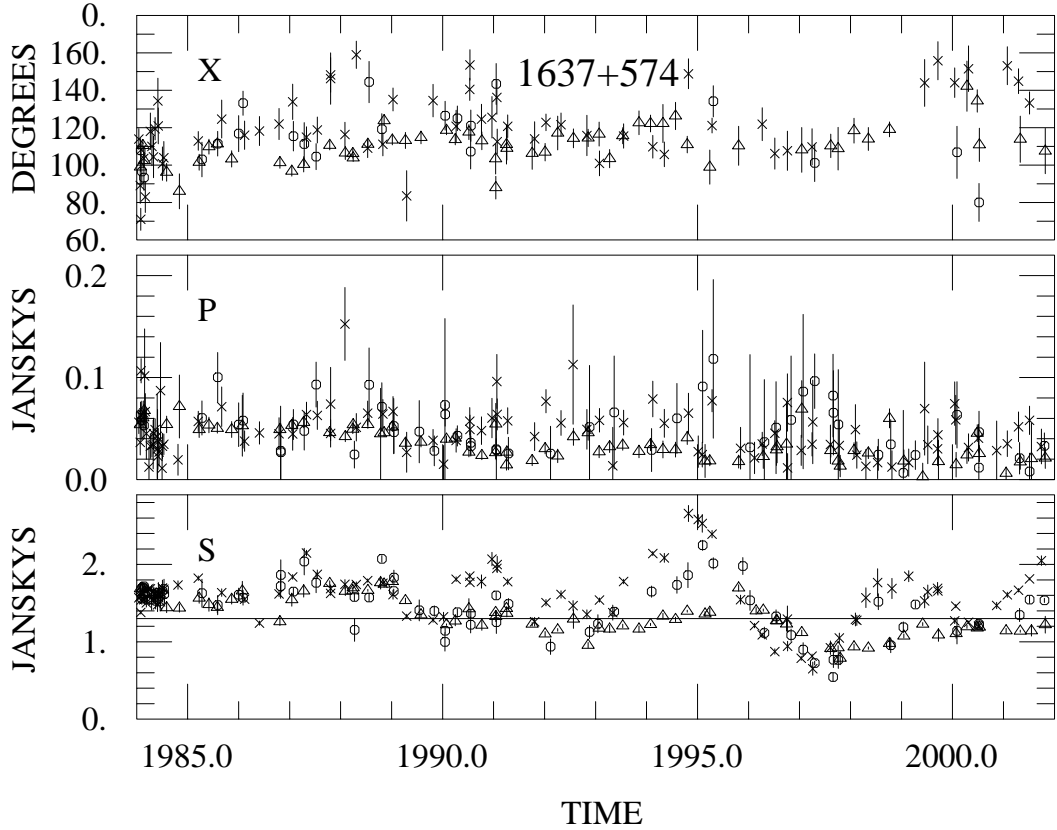


Fig. 5.— From bottom to top, daily averages of the total flux density, polarized flux, and EVPA for the flat spectrum QSO 1637+574. The observations at 14.5, 8.0 and 4.8 GHz are denoted by Xs, circles, and triangles respectively, and the polarization has been corrected for Faraday rotation assuming a rotation measure of $+22 \text{ rad m}^{-2}$. The symbol convention is adopted in all of the subsequent light curves. The solid line in the lower panel marks the 1.3 Jy total flux density level used as a selection criterion for the sample. The source has exhibited a series of well-defined events occurring every few years with a flat to inverted spectrum.

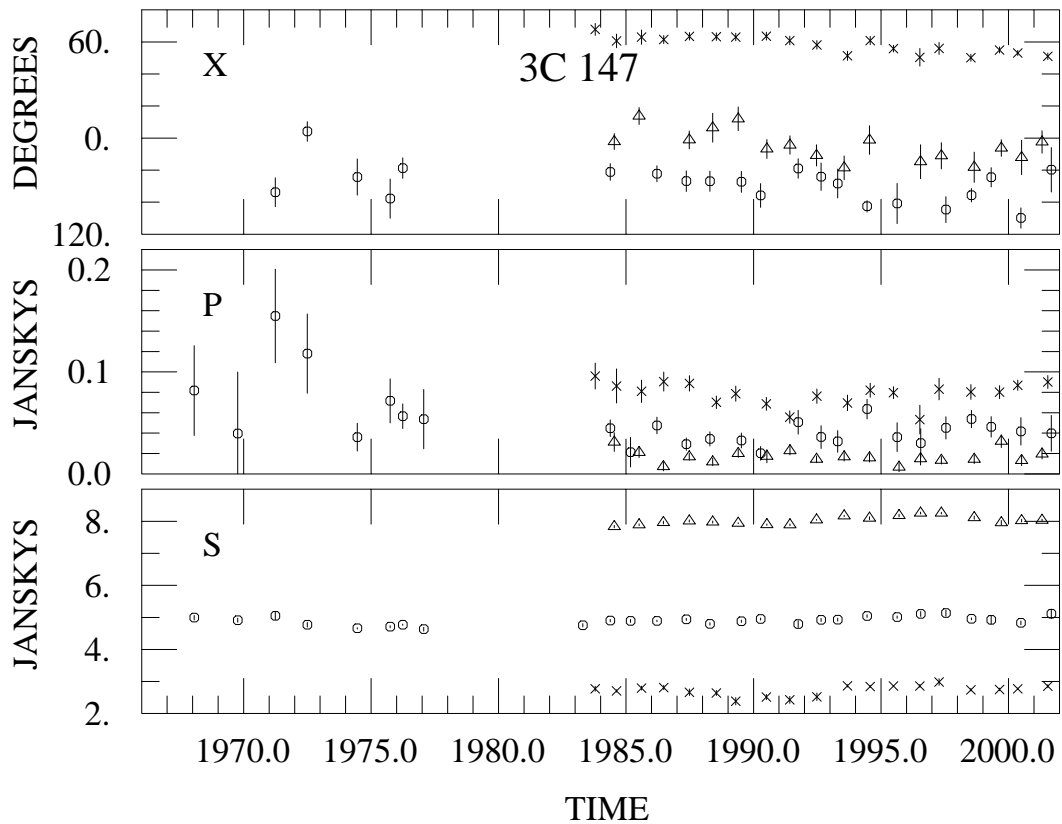


Fig. 6.— Yearly averages of the total flux density, polarized flux, and EVPA for the steep spectrum QSO 0538+498 (3C 147). The symbols are as denoted in Figure 5.

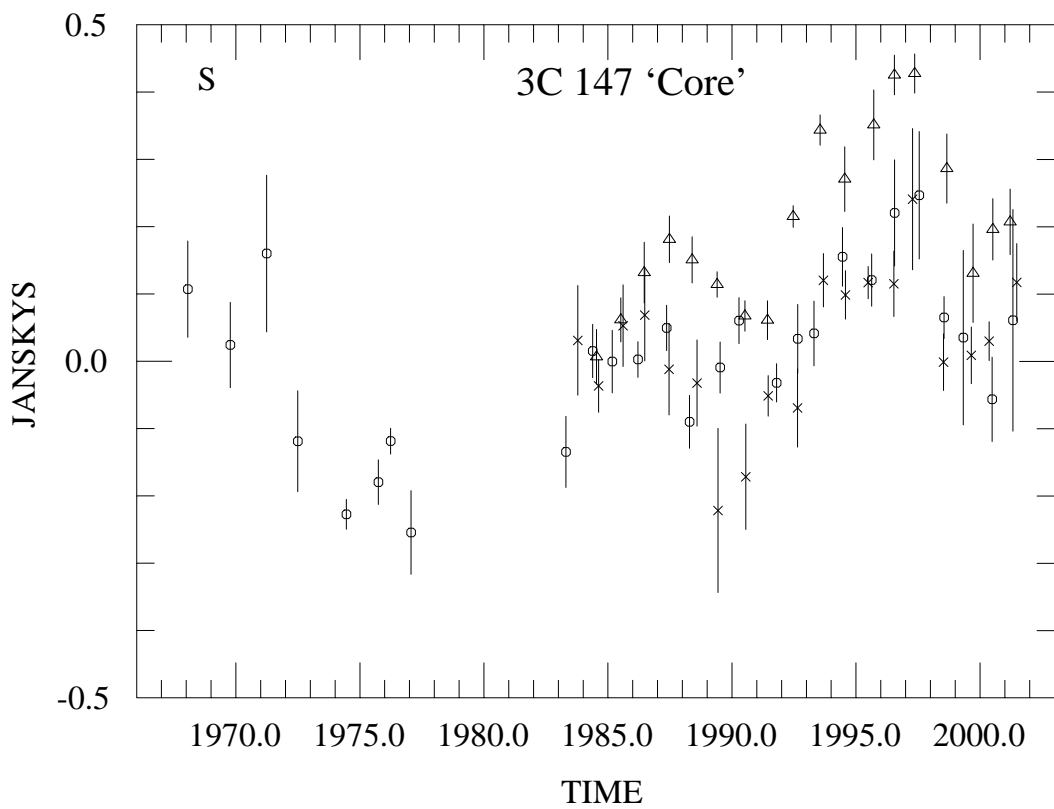


Fig. 7.— A blow-up showing flux density only for 3C 147, with baseline fluxes removed as specified by the spectrum given in Ott et al. (1994).

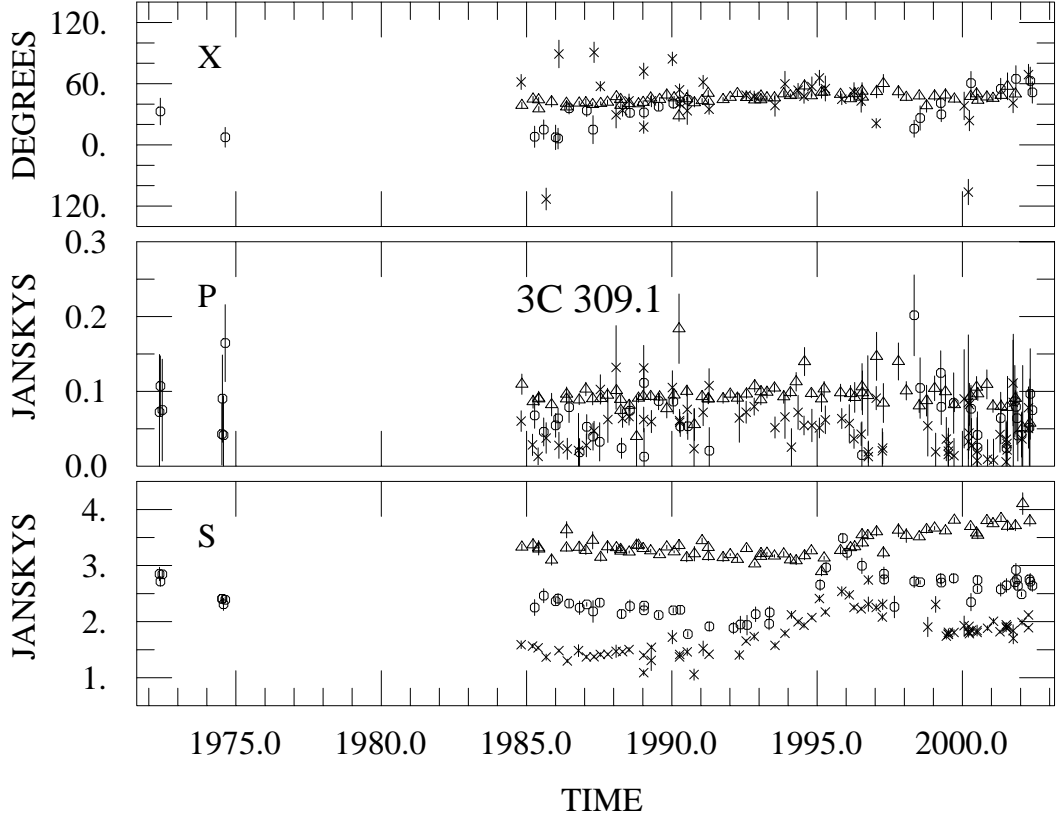


Fig. 8.— From bottom to top, daily averages of the total flux density, polarized flux, and EVPA for the steep spectrum compact object 1458+718 (3C 309.1). The full time range of our data is shown. Although undersampled, variations clearly occurred during the mid 1970s, as well as in the mid 1990s. The polarization has been corrected for Faraday rotation assuming a rotation measure of 75 rad m^{-2} . This integrated RM differs slightly from the value of 60 rad m^{-2} given by Aaron, Wardle, and Roberts (1998) and discussed in the text.

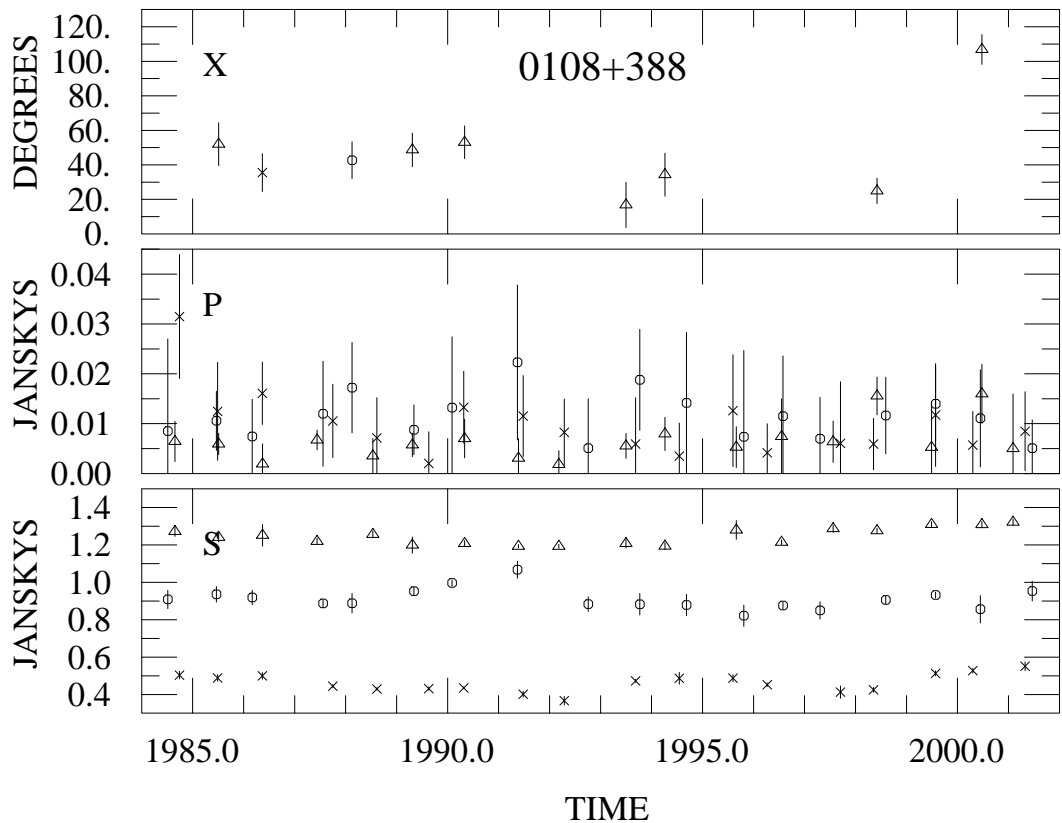


Fig. 9.— From bottom to top, yearly averages of the total flux density, polarized flux, and EVPA for the compact symmetric, GHz-peaked galaxy 0108+388. The low degree of variability is typical of that seen in other csos, and the total flux density spectrum is characteristic of GHz-peaked objects. The spectral turnover at 3.9 GHz in this object (Stangellini et al. 1998), is outside the range of our spectral coverage.

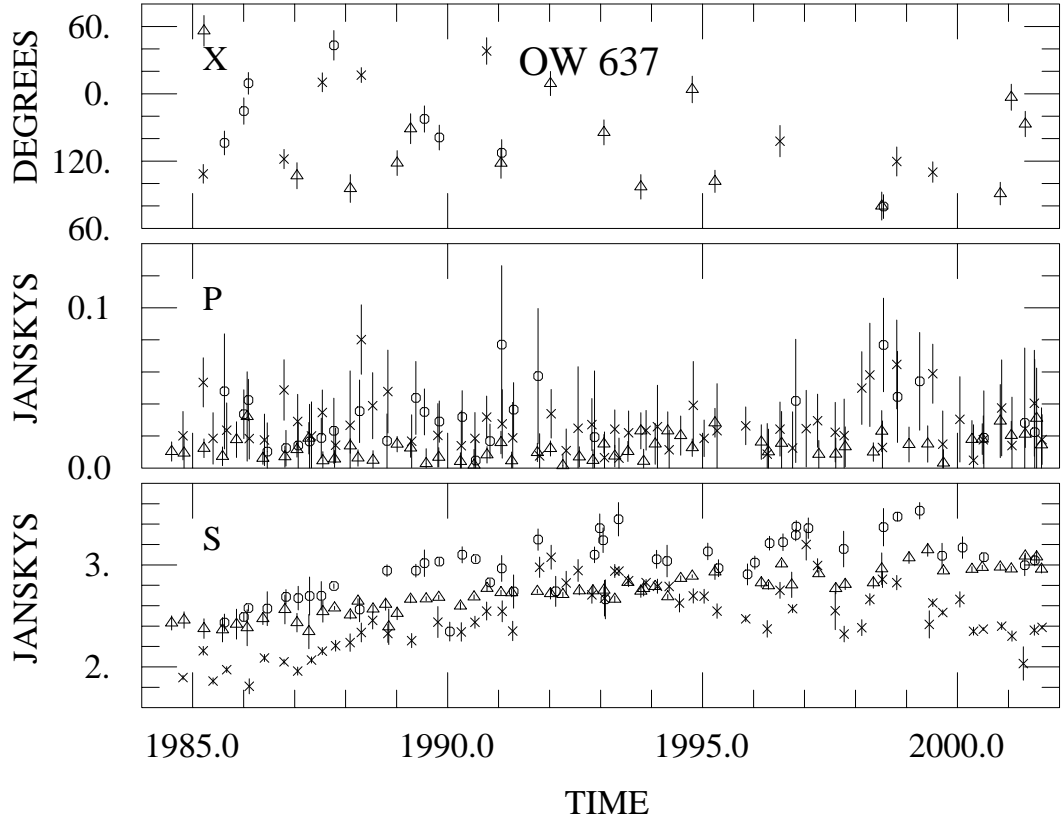


Fig. 10.— From bottom to top, monthly averages of the total flux density, polarized flux, and EVPA for the COINS sample member 2021+614. The polarization has been corrected for Faraday rotation assuming a rotation measure of -99 rad m^{-2} ; few values of EVPA are shown because most are below our signal-to-noise criterion for inclusion. The spectral turnover, at 8.4 GHz (Stangellini et al. 1998), is within our spectral coverage. The source exhibits well-defined variability while maintaining its GPS spectral shape.

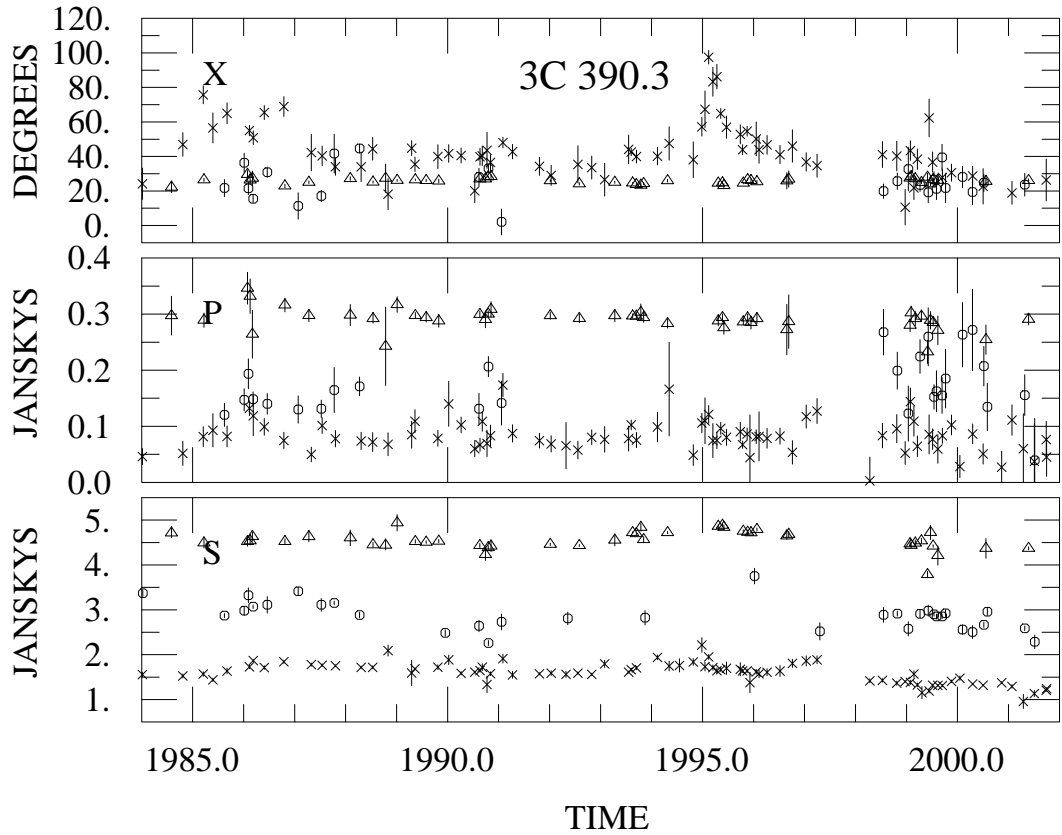


Fig. 11.— From bottom to top, monthly averages of the total flux density, polarized flux, and EVPA for the X-ray bright galaxy 3C 390.3. The EVPA (top panel) has remained stable at 4.8 GHz, but it shows at least one large swing at 14.5 GHz. The monthly averaging has smoothed out the short term activity at 14.5 GHz in both total flux density and polarization.

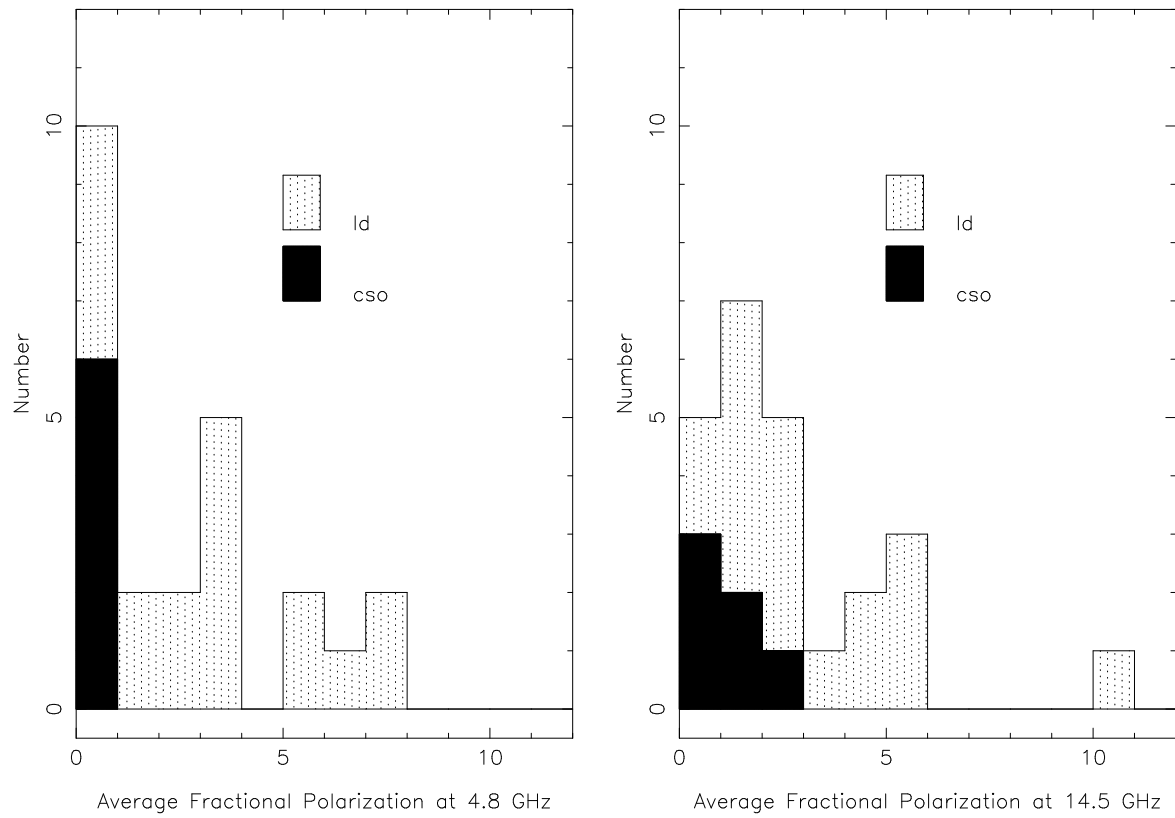


Fig. 12.— Histogram of average fractional polarization based on the data at 4.8 GHz (left) and at 14.5 GHz (right) for the steep spectrum radio classes compact symmetric (cso) and lobe-dominated (ld).

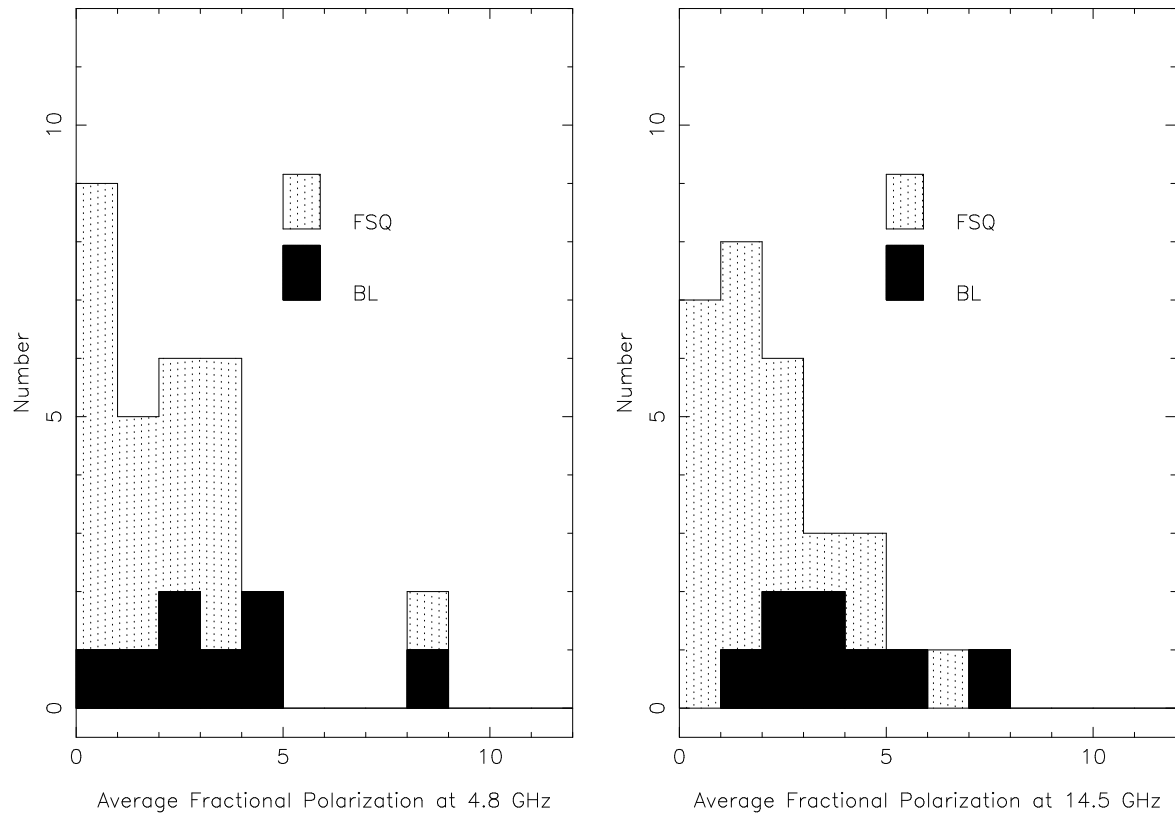


Fig. 13.— Histogram of average fractional polarization based on the data at 4.8 GHz (left) and 14.5 GHz (right) for the flat spectrum QSOs and BL Lacs.

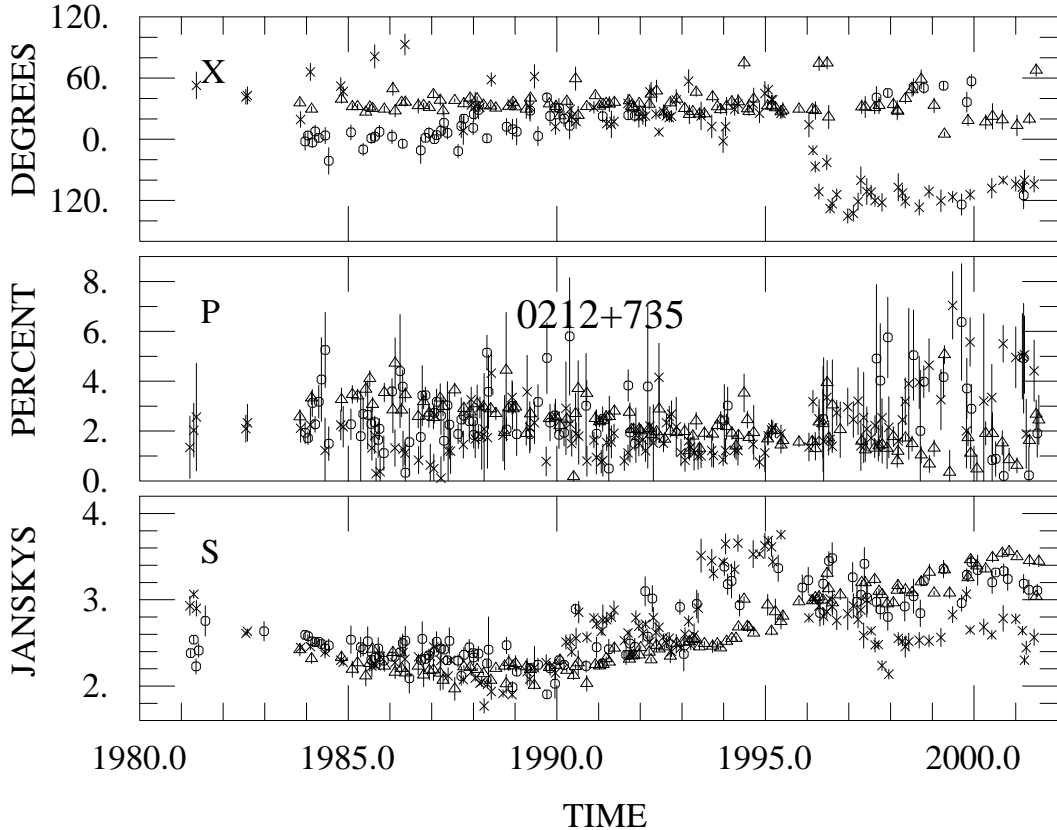


Fig. 14.— Monthly averages of the total flux, fractional polarization, and EVPA for the variable, high-redshift QSO 0212+738. A dramatic change in the behavior of the EVPA commenced in 1996 when the orientation of the EVPA at 14.5 GHz aligned with the orientation of the flow direction (B perpendicular to the flow). During this time period the fractional polarization increased significantly at 8.0 and 14.5 GHz and decreased at 4.8 GHz. Note also the decrease in the total flux at 14.5 GHz during the same time period.

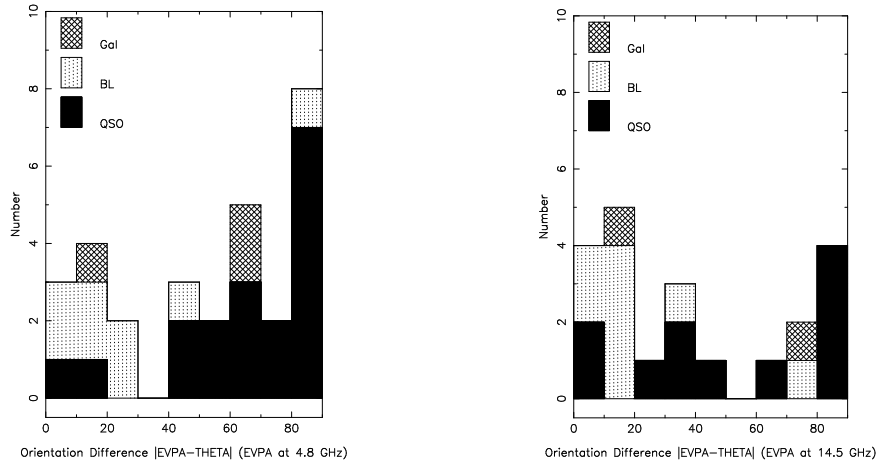


Fig. 15.— Left: orientation difference between the preferred EVPA at 4.8 GHz and the flow direction indicated by the observation of θ at the highest VLBI frequency given in Table 2 for each source. Right: orientation difference based on the preferred EVPA at 14.5 GHz and the same adopted flow direction. In a transparent synchrotron source the EVPA is orthogonal to the magnetic field direction.

Table 1. SELECTED EMISSION PROPERTIES OF PROGRAM SOURCES.

Source (1)	Name (2)	Opt. (3)	radio (4)	z (5)	V(14.5) (6)	FI(14.5) (7)	FI(4.8) (8)	α_{av} (9)	VLB _{43,15} (10)
0016+731		Q	c	1.781	0.62	0.38	0.32	-0.04	K,L
0040+517	3C 20	G	ld	0.174	0.19	0.06	-0.01	-1.02	
0108+388	OC 314	G	cso	0.668	0.25	0.09	0.04	-0.91	
0133+476	DA 55	Q	c	0.859	0.71	0.39	0.29	+0.27	K,L
0153+744		Q	cd	2.338	0.31	0.14	0.09	-0.93	K,L
0212+735		Q	a1	2.367	0.31	0.16	0.15	+0.03	K,L
0220+427	3C 66B	G	ld	0.021	0.30	0.14	0.03	-1.32	
0315+416	3C 83.1B	G	ld	0.025	0.34	0.13	0.04	-1.10	
0316+413	3C 84	G	i	0.018	0.49	0.29	0.34	-0.19	L
0404+768	4C 76.03	G	cso	0.599	0.12	0.04	0.01	-0.60	
0538+498	3C 147	Q	ssc	0.545	0.26	0.10	0.01	-0.98	L
0605+480	3C 153	G	ld	0.277	0.10	-0.02	0.03	-1.08	
0710+439	OI 417	G	cso	0.518	0.11	0.03	0.03	-0.64	K
0711+356	OI 318	Q	cd	1.62	0.27	0.07	0.12	-0.67	L
0723+679	3C 179	Q	ld	0.846	0.47	0.14	0.07	-0.35	L
0804+499	OJ 508	Q	c	1.43	0.64	0.30	0.24	+0.05	K,L,J
0809+483	3C 196	Q	ld	0.871	0.18	0.03	0.01	-1.15	
0814+425	OJ 425	BL	c	0.245	0.57	0.34	0.22	-0.06	K,L
0831+557	4C 55.16	G	i	0.242	0.24	0.12	0.00	-1.11	
0836+710	4C 71.07	Q	a2	2.172	0.47	0.26	0.09	-0.25	K,L,J
0850+581	4C 58.17	Q	c	1.322	0.20	0.09	0.03	-0.40	K,L
0859+470	4C 47.29	Q	a1	1.462	0.26	0.12	0.09	-0.29	L
0906+430	3C 216	Q	ssc	0.670	0.22	0.08	0.04	-0.40	L
0917+458	3C 219	G	ld	0.174	0.17	0.04	0.03	-1.21	
0923+392	4C 39.25	Q	cd	0.695	0.58	0.45	0.24	-0.05	K,L
0945+408	4C 40.24	Q	a2	1.252	0.32	0.20	0.21	-0.15	K,L
0951+699	M 82	G	...	0.001	0.12	0.06	0.01	-0.68	
0954+556	4C 55.17	Q	...	0.909	0.24	0.10	0.02	-0.41	L
0954+658		BL	...	0.368	0.82	0.38	0.49	+0.04	L,J
1003+351	3C 236	G	ld	0.101	0.17	0.08	0.04	-0.61	
1031+567	OL 553	G	cso	0.460	0.35	0.15	0.03	-0.97	
1157+732	3C 268.1	G	ld	0.970	0.13	0.06	0.02	-0.91	
1254+476	3C 280	G	ld	0.996	0.12	0.03	0.03	-1.05	
1358+624	4C 62.22	G	cso	0.431	0.18	0.05	0.02	-0.84	
1409+524	3C 295	G	ld	0.464	0.12	0.02	0.02	-1.24	
1458+718	3C 309.1	Q	ssc	0.905	0.38	0.19	0.05	-0.59	K
1609+660	3C 330	G	ld	0.550	0.15	0.05	0.02	-1.17	
1624+416	4C 41.32	Q	a2	2.550	0.30	0.17	0.11	-0.39	L
1633+382	4C 38.41	Q	a2	1.814	0.33	0.15	0.13	-0.16	K,L,J
1634+628	3C 343	Q	ssc	0.988	0.20	0.11	0.02	-1.24	
1637+574	OS 562	Q	c	0.751	0.54	0.27	0.18	+0.16	L
1641+399	3C 345	Q	a2	0.593	0.47	0.26	0.24	+0.02	K,L
1642+690	4C 69.21	Q	c	0.751	0.43	0.14	0.13	+0.00	K,L
1652+398	Mkn 501	BL	a2	0.034	0.20	0.07	0.09	-0.25	K,L,J
1739+522	4C 51.37	Q	c	1.375	0.71	0.46	0.51	+0.00	K,L,J
1749+701		BL	a1	0.770	0.41	0.17	0.11	-0.16	K,L
1803+784		BL	a1	0.680	0.31	0.12	0.13	+0.03	K,L
1807+698	3C 371	BL	a2	0.051	0.32	0.14	0.09	-0.12	K,L

Table 1—Continued

Source (1)	Name (2)	Opt. (3)	radio (4)	z (5)	V(14.5) (6)	FI(14.5) (7)	FI(4.8) (8)	α_{av} (9)	VLB _{43,15} (10)
1823+568	4C 56.27	BL	a1	0.664	0.42	0.21	0.10	+0.09	K,L
1828+487	3C 380	Q	ssc	0.692	0.18	0.09	0.05	-0.56	K,L
1842+455	3C 388	G	ld	0.091	0.14	0.04	0.02	-1.02	
1845+797	3C 390.3	G	ld	0.056	0.19	0.12	0.04	-0.94	K
1928+738	4C 73.18	Q	a1	0.302	0.24	0.11	0.06	-0.09	K,L
1939+605	3C 401	G	ld	0.201	0.17	0.02	0.03	-1.11	
1954+513	OV 591	Q	a1	1.220	0.48	0.27	0.13	-0.10	K,L
2021+614	OW 637	Q	cso?	0.227	0.22	0.13	0.05	-0.09	K,L
2153+377	3C 438	G	ld	0.290	0.19	-0.04	0.03	-1.30	
2200+420	BL LAC	BL	a1	0.069	0.59	0.32	0.27	-0.02	K,L,J
2229+391	3C 449	G	ld	0.017	0.23	0.08	0.04	-1.27	
2243+394	3C 452	G	ld	0.081	0.35	0.08	0.02	-1.48	
2351+456	4C 45.51	Q	a2	1.992	0.46	0.25	0.16	-0.17	L
2352+495	DA 611	G	cso	0.237	0.14	0.05	0.03	-0.69	

Table 2. POLARIZATION AND SMALL-SCALE STRUCTURE ORIENTATIONS.

Source (1)	RM (2)	Ref (3)	P% _{av} (14.5) (4)	sd (5)	χ_0 (14.5) (6)	% (7)	χ_0 (4.8) (8)	% (9)	Θ_5 (10)	Ref (11)	Θ_{15} (12)	Ref (13)	Θ_{43} (14)	Ref (15)
0016+731	-3	Ru	1.36	0.16	np		66	25	156	P1	u	KZ	132	L
0040+517	+159	SN	1.88	0.15	57	16	19	38	wc	P1
0108+388	+3	Ru	0.44	0.37	np		np		237	P1
0133+476	+28	RJ	0.15	0.08	np		22	35	317	W	321	KZ	330	L
0153+744	-42	Ru	3.82	0.43	np		np		156	P1	101	KZ	68	L
0212+735	+14	Ru	0.69	0.09	30	25	33	77	103	P1	111	KZ	121	L
0220+427	...		2.79	0.28	np		71	98
0315+416	+18	SN	4.27	0.41	115	27	105	98	90	Xu
0316+413	+76	Ru	0.12	0.01	14	19	11	18	190	W	190	HW	176	L
0404+768	...		2.79	0.24	42	39	np		48	P1
0538+498	-1300	Na	2.77	0.07	91	81	np		230	P1	237	L
0605+480	+34	SN	5.88	0.51	np		45	95	wc	P1	112	KZ
0710+439	-7	Ru	0.50	0.32	np		np	0	P1
0711+356	+40	St	1.09	0.37	np		np		338	P1	329	L
0723+679	-25:	Ru	0.98	0.36	np		177	78	272	P1	256	L
0804+499	+2	Ru	1.40	0.13	np		85	46	115	XP	130	KZ	127	L
0809+483	-142	SN	1.40	0.17	np		153	100	wc	P1
0814+425	+19	Ru	2.40	0.17	92	35	83	40	130	GP	84b	KZ	103	L
0831+557	+113	Ru	0.49	0.14	np		np		292:	P1
0836+710	-11	W1	4.67	0.15	106	76	105	100	214	P1	201	L
0850+581	-6	Ru	4.07	0.29	69	29	np		156	P1	176	KZ	227	L
0859+470	-31	RJ	1.55	0.31	np		92	80	4	XP	357	L
0906+430	+28	RJ	0.82	0.14	np		84	80	155c	P1	151	L
0917+458	-19	SN	2.86	0.30	np		148	94	wc	P1
0923+392	+15	RJ	2.73	0.08	134	83	110	55	277	P1	278	KZ	93	L
0945+408	+7	RJ	1.34	0.16	np		15	98	127c	P1	u	KZ	137	L
0951+699	...		1.24	0.17	np		171	38	240	P1
0954+556	+1	SN	3.98	0.19	5	67	4	94	191	L
0954+658	-15	Ru	4.88	0.24	166	39	175	72	306	P1	311	L
1003+351	-4	Ru	0.79	0.33	np		107	18	292	P1
1031+567	...		0.65	0.55	np		np
1157+732	+8	SN	5.00	0.38	115	43	143	79	wc
1254+476	-17	SN	10.99	0.37	54	78	48	100	wc
1358+624	...		1.64	0.23	np		np		305:	P1
1409+524	...		1.56	0.10	105	21	np		wc	P1
1458+718	+75:	Ru	2.20	0.23	50	38	46	98	164c	P1

Table 2—Continued

Source (1)	RM (2)	Ref (3)	P% _{av} (14.5) (4)	sd (5)	χ_0 (14.5) (6)	% (7)	χ_0 (4.8) (8)	% (9)	Θ_5 (10)	Ref (11)	Θ_{15} (12)	Ref (13)	Θ_{43} (14)	Ref (15)
1609+660	+13	SN	3.88	0.35	np		129	94	wc	P1	
1624+416	+1	Ru	1.01	0.27	np		np	239c	P1	...		262	L	
1633+382	+15	RJ	0.24	0.08	np		15	42	295	P1	282	KZ	279	L
1634+628	+0	Ru	2.36	0.49	np		55	20	
1637+574	+22	RJ	2.28	0.15	118	50	111	76	190	XP	...		200	L
1641+399	+29	RJ	1.52	0.07	37	61	24	94	230c	P1	270	KZ	284	L
1642+690	-11	W1	6.38	0.16	159	80	116	32	195	P1	195b	KZ	158	L
1652+398	+42	Ru	2.22	0.14	178	48	177	37	130	P1	147b	KZ	160	L
1739+522	-4	Ru	1.07	0.13	np		np	25	XP	...		204	L	
1749+701	+ 8	W1	5.04	0.28	85	23	89	38	296c	P1	301c	KZ	275	L
1803+784	-61	W1	3.42	0.09	98	70	91	80	268c	P1	267c	KZ	291	L
1807+698	+200	Wr	1.75	0.08	151	22	162	75	263	P1	263	KZ	252	L
1823+568	+36	W1	7.30	0.17	29	86	29	96	197c	P1	202c	KZ	201	L
1828+487	+26:	Ru	0.74	0.07	np		30	98	328	P1	...		311	L
1842+455	...		1.54	0.31	np		174	87	wc	P1	
1845+797	-5	SN	4.39	0.19	41	66	27	100	322	P1	324	KZ	...	
1928+738	+33	W1	2.44	0.06	79	79	79	98	166	P1	163	KZ	166	L
1939+605	...		2.02	0.42	np		35	87	wc	P1	
1954+513	...		0.99	0.20	np		np	294	XP	...		307	L	
2021+614	-99	Ru	0.00	0.09	np		np	33	P1	31	KZ	214	L	
2153+377	...		2.80	0.47	np		np	wc	P1		
2200+420	-205	RJ	3.66	0.10	37	63	41	70	188	P1	189	KZ	209	L
2229+391	-162	SN	1.72	0.55	np		106	92	wc	P1	
2243+394	-274	RZK	5.75	0.35	177	39	3	98	82	P1	
2351+456	-12:	Ru	2.27	0.19	110	34	80	41	298	P1	...		321	L
2352+495	...		1.21	0.31	np		np	339	P1		

References. — RM notes: (Na) Nan et al. (2000); (RJ) Rudnick and Jones (1983); (Ru) Rusk (1988); (RZK) Rudnick et al. (1983); (SN) Simard-Normandin et al. (1981); (St) Stangellini et al. (1998); (W1) Wrobel (1993); (Wr) Wrobel (1987).

Theta: (GP) Gabuzda, Pushkarev, & Cawthorne (2000); (KZ) Kellermann et al. (1998): measured from maps at www.cv.nrao.edu/2cm survey; (L) Lister (2001a); (HW) measured from maps in Homan & Wardle (1999); (P1) See paper 1, Aller, Aller, and Hughes (1992); (W) Wehrle et al. (1996); (Xu) Xu, O'Dea, & Biretta (1999); (XP) Xu, W. & Polatidis, A. Private Communication.

Note. — RM notes. 3C 295: our data are consistent with a large, time-variable RM. 3C 371: the value adopted differs from that in Aller, Aller, and Hughes (1992). A range of values exists in the literature for this source. We have used the value which is most consistent with our data. 1928+738: Taylor (2000) finds a position-dependent RM. Our frequency-dependent spread is not consistent with the large RM he finds for component A. BL Lac: we use the value given in Rudnick and Jones (1983); recent VLBA observations suggest that this source property is time variable (Mutel and Denn 2000; Reynolds et al. 2001).

Theta notes. We adopt the value indicative of the inner flow. Most jets are kinked or bent. b & c flag structure showing sharp bends or curved structure. In these cases the flow direction is highly-position dependent. 3C 83.1: source exhibits twin jets on parsec scales.

Table 3. Polarization Spectra of Lobe-Dominated Objects.

Source (1)	opt. class (2)	P(%) _{av(14.5)} (3)	P(%) _{av(4.8)} (4)	Pol. Spectrum (5)	FR class (6)	l (kpc) (7)
0040+517	G	1.88	0.50	F/I	II	202.3
0220+427	G	2.79	3.59	S	I	[90]
0315+416	G	4.27	5.88	S	I	[36]
0605+480	G	5.88	3.97	S/F	II	37.7
0723+679	Q	0.98	3.78	F	II	124.7
0809+483	Q	1.40	2.32	S	II	45.1
0917+458	G	2.86	3.20	S	II	553.4
1003+351	G	0.79	0.70	I	II	5853.3
1157+732	G	5.00	1.73	F/I	II	365.0
1254+476	G	10.99	7.60	S	II	109.8
1409+524	G	1.56	0.04	I/F	II	32.3
1609+660	G	3.88	3.59	S/F	II	450.2
1842+455	G	1.54	1.68	S/F	II	70.4
1845+797	G	4.39	6.40	S	II	315.2
1939+605	G	2.02	2.04	F/S	II	80.5
2153+377	G	2.80	0.35	I	II	102.4
2229+391	G	1.72	5.82	S	I	[38]
2243+394	G	5.75	7.10	S	II	534.1

Table 4. Orientation Difference for BL Lacs.

Source	$ \chi_0(4.8) - \theta_{15} $	$ \chi_0(4.8) - \theta_{43} $	$ \chi_0(14.5) - \theta_{15} $	$ \chi_0(14.5) - \theta_{43} $
0814+425	1	20	8	11
0954+658	...	44	...	35
1652+398	30	17	31	18
1749+701	32	6	36	10
1803+784	4	20	11	13
1807+698	79	90	68	79
1823+568	7	8	7	8
2200+420	32	12	28	8